

STATISTICAL MECHANICS AND DYNAMICS OF THE OUTER SOLAR SYSTEM. 1. THE JUPITER/SATURN ZONE

Kevin R. Grazier^{1,2}, William I. Newman^{1,3}, William M. Kaula^{1,4},
and James M. Hyman⁵

Abstract: We report on numerical simulations designed to understand how the solar system evolved through a winnowing of planetesimals accreted from the early solar nebula. This sorting process is driven by the energy and angular momentum and continues to the present day. We reconsider the existence and importance of stable niches in the Jupiter/Saturn zone using greatly improved numerical techniques based on high-order optimized multi-step integration schemes coupled to roundoff error minimizing methods. We repeat the investigations of Weibel et al. (1990) with one hundred thousand massless particles—nearly 103 times more particles than our 1990 investigation. The increase in the numbers of test particles facilitates robust statistical inference and comparison with analytic results derived from statistical mechanics and kinetic theory. The primordial planetesimal swarm evolved in a phase space divided into regimes by separatrices which define their trajectories and fate. We observed three stages in the planetesimal dynamics. At the start of the simulation many planetesimals are quickly eliminated by the activity spheres of Jupiter or Saturn. Next there is a gravitational relaxation phase where the surviving particles are exponentially eliminated by random gravitational encounters with Jupiter or Saturn. Finally, the only long-lived particles in the simulation were initially located at either a Lagrange point or in an orbit commensurable with Jupiter or Saturn. By comparing the simulation with earlier investigations, we verified the role that Hamiltonian chaos may have played in previous studies. We conclude that niches for planetesimal material are rare and only extremely high accuracy long simulations with many particles will be able to capture even the qualitative nature of early solar system planetesimal evolution.

1. INTRODUCTION

The solar system is a paradigm for dynamical complexity that is reluctant to

1. "Department of Earth and Space Sciences, University of California, Los Angeles, CA 90095."

2. The Jet Propulsion Laboratory, California Institute of Technology, Pasadena, CA 91109.

3. Departments of Physics and Astronomy, and Mathematics, University of California, Los Angeles, CA 90095.

4. Institute of Geophysics and Planetary Physics, University of California, Los Angeles, CA 90095.

5. Theoretical Division, Los Alamos National Laboratory, Los Alamos, NM 87545.

reveal the secrets behind its origin and evolution. Planetesimals formed from the solar nebula that accreted to form the planets underwent a winnowing according to their energy, angular momenta, and phase angles. This sorting process continues to the present day because there still exist planetesimals with marginally chaotic orbits. The dynamical phase space describing the early solar system, as well as today's, is divided into regimes by separatrices which define the planetesimals' trajectories and fate. The solar system we see today is the product of this dynamical complexity. The remaining planetesimals hold clues to its origin and evolution.

Observable planetesimals are absent from most candidate niches in the outer solar system. Giorgini et al. (1996) have compiled a database for all solar system bodies for which the orbits are well-determined. The solutions for the orbital element S for this database come from three sources: the Minor Planet Circulars, published by the IAU Minor Planet Center at the Harvard-Smithsonian Center for Astrophysics (Marsden, 1996), the Lowell Observatory Database of Asteroid Orbits (Bowell, 1996) and the Jet Propulsion Laboratory Solar System Dynamics Group (Donald K. Yeomans, supervisor). Of the bodies from the JPL database, only 165 have semimajor axes which place them in the Jupiter/Saturn zone, and of the more than 100⁰⁰ asteroids in this list, all but one are Trojan asteroids- situated at the leading and trailing Lagrange points of Jupiter. The lone exception is 944 Hidalgo, which crosses both the orbits of Jupiter and Saturn. Additionally, there are also observed approximately 25 comets whose semimajor axes lie between those of Jupiter and Saturn, and all but one cross Jupiter's or Saturn's orbits, or both. This one exception, P/Schwassmann-Wachmann 1, has a semimajor axis of 6.041 AU and an eccentricity of 0.045. It is not easy to extrapolate from this one observable Jupiter/Saturn zone object to include smaller objects that would be visible had they been in the relatively nearby asteroid belt. Nevertheless, the observation of only one possibly long-lived Jupiter/Saturn object, in contrast with the order

of 1 0,000 asteroids between Mars and Jupiter, provides a compelling observational case for assuming that the Jupiter/Saturn zone is highly depleted.

Does the apparent absence of such bodies indicate the presence of primordial processes at a time when the formation of the planets was not yet complete, or are we seeing evidence for an evolutionary process where early solar system bodies on the edge of chaos (Newman et al., 1995), exposed to qualitative bifurcations in their dynamics, were removed from all regions in the outer solar system?

This paper and its sequel describe a massive simulation effort designed to unravel some of these questions. Building upon earlier work by many investigators, we seek to explore the nature of various niches situated throughout the outer solar system. In this paper, we return to the region between Jupiter and Saturn, allowing for trajectories with significant inclination, to better understand the fate of material situated in this regime. In the sequel, we will explore the regions between Saturn and Uranus, as well as Uranus and Neptune.

We have developed integration methods more precise than any previously applied to this problem. The methods used are *exact* up to double precision computer accuracy and the sole source of error is due to the cumulative effect of roundoff. Our numerical technique can be regarded as a refinement of existing methods that had been widely used by dynamicists for decades—see §3. In particular, our contribution to the methodology has made the accuracy formerly available only on special-purpose computers [i.e. the Digital Orrery exploited by Sussman and Wisdom (1988)], accessible to anyone with access to modern workstations. Further, we have performed the computations to minimize the accrued roundoff so that such error will not unnecessarily contaminate the outcome of our investigation. We have performed our investigations over a period of 10^9 years, a period extending well beyond the early dynamical evolution of the solar system. Nevertheless, we have validated our integration schemes by showing that longitude errors in the major

planets grow no faster than the time $t^{3/2}$ and the uncertainty in their positions after one billion years is less than 1 0. To preserve the essential physics of solar system origin, our investigations have been fully three-dimensional and incorporate the full gravitational effect, of all of the Jovian planets: Jupiter, Saturn, Uranus and Neptune. The effect of the terrestrial planets on the depletion of outer solar system niches is negligible due to their small mass and high orbital frequencies- apart from their time-averaged influence- therefore we incorporated their masses into that of the Sun. Relativistic and non-gravitational effects are also ignored.

Thus, the first major difference between the present investigations and that of its predecessors resides in its vastly improved accuracy. This, of course, had the price of increased computational time, but we *were* able to exploit the availability of 161 high-performance Hewlett-Packard workstations in the execution of this project (50 workstations were used in the sequel). Our methodology is also, to use the term commonly employed by computer scientists, "embarrassingly parallel" and directly computable on the new generation of massively parallel computers.

These highly accurate simulations can be used as a benchmark against which we test other approximate integration schemes. Our integration scheme, since it is exact to machine precision, is *a posteriori* symplectic, using the definition of Feng (1987, 1995). Significantly, we have found qualitative differences between our results and those obtained by other investigators who employed less accurate symplectic integrators. It is noteworthy, in the numerical analysis and symplectic methods literature, that others have confirmed the problems of using symplectic methods- especially those employing large step sizes- in nearly-chaotic environments. See Sanz-Serna and Calvo (1994) for a review.

More recently, Lessnick (see Haberkorn, 1996), in her dissertation, has shown that symplectic methods can cause planetesimals traveling in the neighborhood of separatrices, which distinguish qualitatively different dynamical regimes, to undergo

non-physical bifurcations in their behavior. Lesnick also showed that symplectic methods applied to Hamiltonian systems can make integrable problems—such as the two-center problem and the Stark effect problem—appear chaotic. We will present in a future paper the results of a detailed practical investigation into the differences between symplectic and multistep integrators (Grazier et al. 1996; Haberkorn et al. 1996).

Another major difference between this work and that of its predecessors is the role of statistics and the application of kinetic theory. Earlier work by ourselves, and many other groups, considered hundreds of particles in limited surveys of these niches, and provided important insights into these processes. However, firm conclusions cannot be drawn from these initial efforts due to the “statistics of small numbers” (Newman et al., 1989, 1992, 1994). An essential feature to be remembered from simple random walk arguments is, for situations composed of N “events,” that the prevailing uncertainty is of order $N^{1/2}$ (Chandrasekhar, 1943). Accordingly, the relative uncertainty is of order $N^{-1/2}$ which renders surveys with only hundreds of events to be inadequate for precise statistical inference. (Mel-cm, there could exist narrow niches of stability that would be missed by coarse surveys.)

We have employed more than 100,000 test particles in the present survey of the Jupiter/Saturn zone and, in this paper’s sequel, 10,000 each in the Saturn/Uranus and Uranus/Neptune zones. As a consequence, we are in a position for the first time to draw statistically reliable conclusions from our investigations. While these statistical results offered no fundamental surprises, they did show some order-of-magnitude quantitative difference with earlier work, for example in the particle depletion rate found in these niches.

However, as we will shortly show, our dramatically improved statistics allow us to show one aspect of Hamiltonian chaos never before observed in solar system investigations, the possible imprint of a “fractal” geometry (formally known

as “fractal basin boundaries,” see for example Ott, 1993) in the ultimate fates of the test particles. Given the reliability of our statistics, we felt it important that we develop a statistical mechanical or kinetic theory which would provide an *ab initio* confirmation of our results. Here, we build on the theory developed by Chandrasekhar (1943) in stellar dynamics, Spitzer (1962) in plasma physics, and Stewart and Wetherill (1988) in solar system dynamics, incorporating the geometry of these solar system niches. This, too, we have done providing further confirmation of our nonlinear dynamical results.

2.1 PREVIOUS WORK

In 1973 Lecar and Franklin (hereafter referred to as LF73) examined the region from 5.72 AU to 9.10 AU for 6,000 years using a model which integrated initially circular particle orbits, but modeled Jupiter and Saturn analytically. They concluded, had this region initially been populated with planetesimals, that it would quickly be depopulated on a timescale of a few thousand years with the possible exception of two bands at 6.8 AU and 7.5 AU. In the same year Everhart (1973), although primarily interested in Trojan and horseshoe orbits, used a similar model and found two potential long-life bands centered at 7.00 AU and 7.58 AU. While acknowledging that a far more extensive survey was required to gain insight on lifetimes, he felt it probable that no orbits in either of these bands were absolutely stable. Franklin et al. (hereafter referred to as FLS89) extended their work from 15 years earlier, and examined the lifetimes of particles with initially aligned apsidal lines and semi-major axes between 7.0 and 7.5 AU—the long-life bands from LF73 and Everhart (1973). They found that bodies with higher eccentricities, approximating those of their neighboring perturbers, had somewhat longer lifetimes than particles on more circular orbits. FLS89 concluded that it was unlikely that low-inclination bodies survived more than 10^7 years between the two planets, but, noted that bodies on inclined orbits may survive somewhat longer. Duncan et al. (hereafter referred to as

1 (DQT89) developed a two-planet mapping that approximated the restricted three-body problem, and examined the zones between each of the outer planets for up to the lifetime of the solar system (4.5 Gy). In their model, planets were confined to circular, coplanar orbits; test particles had small eccentricities, but were similarly coplanar. Particle orbits were treated as Keplerian, except at conjunctions where they were given an impulsive perturbation and new orbital elements calculated. Between Jupiter and Saturn, DQT89 found that all orbits became planet-crossing within 10^7 years; most were planet-crossing within 10^6 years. Finally, they noted that the "stable" bands at 6.8 and 7.5 AU from LF73 were probably unstable for durations greater than 10^6 years.

Employing a three-dimensional model in which the Sun, Jupiter, and Saturn interacted fully, Weibel et al. (1990)- hereafter referred to as WKN90- integrated the trajectories of 25 test particles, using a sixth order Aarseth (1972) and Ahmad and Cohen (1973) scheme. Confining their integration to low-inclination, low eccentricity orbits in the range from 5.7 to 8.8 AU, they found that all but three particles became planet-crossers within 10^5 years (most within 10^4). WKN90 noted that the longer-lived orbits tended to flank commensurabilities. They also concluded that a truly thorough search for stable orbits in this region required a simulation with much larger ranges in eccentricity and inclinations. Using the same model as LF73, Soper et al. (1990) used the dynamics of the Jupiter/Saturn zone as a backdrop to test how errors in numerical accuracy can effect stable orbits. They also looked to find criteria, short of long integrations, to identify orbits which are potential planet-crossers. Using a fourth-order symplectic mapping, developed by Candy and Rozmus (1990), Gladman and Duncan (1990)- hereafter referred to as GD90- integrated the trajectories of 900 particles between 6.76 and 8.06 AU. In the Gladman and Duncan survey, the Sun, Jupiter, and Saturn were mutually-interacting. This was the first study which used close-approach as a criteria for

removing a particle from the simulation, as opposed to merely planet orbit crossing, as in previous surveys (furthermore they removed any particle leaving the solar system) the introduction of a close approach criterion did not significantly affect their depletion time scale, a result paralleling FLS89. They were also the first to examine the role of non-negligible inclinations on depletion times of particles between Jupiter and Saturn. Both the inclined and invariable plane populations were, they observed, depleted on 10⁵ year time-scales. Finally, Holman and Wisdom (1993) hereafter HW93 used their symplectic mapping technique (Wisdom and Holman, 1991) to survey the invariable plane for stable orbits in the range from 5 to 50 AU. The Sun, and for the first time all of the Jovian planets, were fully-interacting in three dimensions. All test particles were on initially circular orbits. Consistent with previous studies, the majority of their test particles between Jupiter and Saturn were eliminated on 10⁴- to 10⁵ (E-year) time scales (all were removed by 10⁶ years). Of these various investigations, the ones most relevant to the present investigation by virtue of their underlying physical description are WKN90 and GD90 we will focus on the latter in our detailed comparisons. An overview and comparison of previous simulation efforts is given in Table 1.

We now provide a brief description of the computational methods employed (a detailed and mathematically rigorous development of the methods will appear elsewhere), and then go on to provide our results, including comparisons with existing work. In our discussion, we will introduce relevant statistical mechanical derivations and comparisons with our numerical results. Importantly, we will return to the theme of planetesimal dynamics on the edge of chaos and make recommendations germane to future investigations in this field.

3. METHOD

The integration method we employ was first developed by Störmer (1907) to integrate the trajectories of charged particles in a magnetic field (in particular the

Aurora Borealis), and has a well-established pedigree among planetary astronomers. A closely-related methodology was used by Cowell to determine the orbit of Lysithea (the eighth moon of Jupiter), but its more well-known application was by Cowell and Crommelin (1910) to predict the return of comet P/Halley. As is best put by Bate, Mueller, and White (1971), "This method has been 'rediscovered' many times in many forms..." since then (Numerov 1924, 1927; Manning and Millman, 1938). This class of methods went into a dormant state, but saw a resurgence in the mid-1960's through the early 1990's, becoming the standard integration method for celestial mechanics. The Cowell method was used for long-term solar system integrations by Cohen et al. (1965, 1973), but this class of methods reached its highest expression under Applegate et al. (1986) and then Wisdom and Sussman (1988) using the quadruple-precision, parallel-processing Digital Orrery. Both concurrently and subsequently, many other astronomical- and planetary dynamicists have employed this methodology.

The numerical method used in our simulations is a roundoff-minimized truncation-controlled 13th order modified Störmer integrator (Newman et al., 1990, 1993, 1995, 1996; Bell et al., 1994; Goldstein, 1996). The algorithm was expressed in backward-difference, summed-form in order to reduce roundoff accumulation (Hairer et al., 1991). We employed a time step of ≈ 4.24 days which was sufficiently small to guarantee that the computation of any particle trajectory with eccentricity ≤ 0.5 would be *exact* to double precision computer accuracy. Since the integration was exact to machine precision, it can be regarded as *a posteriori* symplectic in the sense of Feng (1987, 1995).

Following procedures routinely employed by computer scientists to minimize the accumulation of roundoff error (e.g. Higham, 1993, 1996) we developed a procedure which we call "significance-ordered computation": where all arithmetic operations are grouped according to the magnitude of the floating point numbers involved,

so that least-significant bit information would not be unnecessarily lost. This arithmetic ordering procedure was employed both in the finite difference computations as well as in the calculation of the gravitational potential and forces.

Henrici (1962) has developed a general theory for the accumulation of error during numerical integrations, distinguishing between systematic and random errors. The latter case, which is optimal in terms of minimizing roundoff error growth, occurs only when all systematic sources of roundoff and truncation error are eliminated. At that point, we can expect the error in normally conserved quantities such as the total system energy) to vary as $t^{1/2}$. Meanwhile, the error in the corresponding "angle" type variables will vary as the integral over time of the former. Hence, the best achievable longitude error growth will vary as $t^{3/2}$. Goldstein (1996) provides a rigorous proof of these scaling laws. Significantly, Quinlan (1994) did not achieve this degree of accuracy owing to his use of a large stepsize and the presence of systematic truncation error (Quinlan, 1995). Previous investigations, which showed energy error linear in time, and longitude error quadratic in time, exhibit the hallmark of systematic error growth.

To test the accuracy of our integration method, we performed two different kinds of tests. First, we performed a limited survey—so that statistics would be available of two-body Kepler problem integrations for 10 million orbits for orbits with eccentricity 0.5 (a problem containing a very wide distribution of time scales compared to more nearly-circular planetary orbits). This test survey was performed using 16 independent runs so that average and root mean squared (RMS) properties of the integrators could be established. Over 16 runs the RMS longitude error after 10 million orbits was 1.4×10^{-3} radians (Fig. 1) and RMS relative energy error 1.0×10^{-11} (Fig. 2). These tests showed that the error in the energy grew as $t^{1/2}$ and the error in the longitude as $t^{3/2}$, where t is the elapsed time. In other words, the accumulated error was as would be expected in the absence of *systematic* error

in the integration scheme.

Further tests of the method were based upon integrations of the outer solar system, adding the mass of the terrestrial planets to that of the Sun. For 16 different sets of initial conditions generated from the JPL245 ephemeris (Standish, 1994), we integrated the trajectories of the Jovian planets for a time interval equivalent to 2^n Jupiter orbits, where n is an integer between 0 and 20. At the end of each integration, we use the positions and velocities of the Sun and planets as starting conditions to integrate *backwards* in time. This forwards/backwards integration represents an excellent test of the integrator's performance in a nonlinear regime.

Fig. 3 shows the relative RMS energy error for the entire system. We can see that the energy error grows as $t^{0.46}$, very nearly $t^{1/2}$, again indicating the absence of systematic error growth. Fig. 4 shows the RMS angular position errors for both Jupiter and Saturn. Given the initial position for a planet \vec{r}_i , and its final position \vec{r}_f , we define the angular position error λ as:

$$\lambda = \arcsin \left(\frac{|\vec{r}_i \times \vec{r}_f|}{|\vec{r}_i||\vec{r}_f|} \right)$$

If our computations had no truncation or roundoff error, we would expect that these forwards/backwards integrations would yield $\vec{r}_i = \vec{r}_f$. Thus, λ is a useful measure of the accumulated error present in these calculations.

We make the distinction between angular position error and true anomaly error since, as we have defined it, the angular position error is referenced to an inertial reference frame, whereas true anomaly error is reference to the perihelion of each planet's orbit—a quantity which is not fixed. We also make the distinction between angular position error and longitude error since the measurement of longitude would involve projecting the angular position error onto the XY plane, (though for low-inclination objects such as Jupiter and Saturn the two are very nearly identical). For the 2-D Kepler Problem in the XY plane as above, longitude error, true anomaly

error, and angular position error are identical

In the N-body tests described in Fig. 4, we see that for both Jupiter and Saturn the angular position error grows at a rate less than $t^{3/2}$, and after 2^{21} Jupiter orbits (nearly 25 million years), the errors for both planets are on the order of 2×10^{-5} radians. These tests manifested a quantitatively similar behavior in the growth of the longitude error obtained in the two-dimensional Kepler problem. A detailed description of this integrator is in Goldstein (1996) and Newman et al. (1996).

The modified Sörmer integrator is a multi-step method (Henrici, 1962; Hairer et al., 1991) and is not self-starting. To start the integration, we used a fourth order Runge-Kutta method combined with Richardson extrapolation (Richardson and Gaunt 1927; Kincaid and Cheney 1991) for the initialization. Initialization was performed in extended (quadruple) precision to eliminate *all* sources of truncation and roundoff error to double precision machine accuracy. By successively halving time steps and invoking Richardson extrapolation, we achieve convergence in our numerical representation of the initial positions to within 5×10^{-17} AU (≈ 7.5 microns!), well below the threshold of physical perturbations in a real solar system caused by objects such as comets and asteroids, solar wind, solar mass loss, and relativistic effects. Our point is simply that we have a particularly effective solution to the initialization problem.

The code for these calculations was developed in the C language and performed on clusters of Hewlett-Packard workstations. Though initial planetary positions were identically preserved across platforms, each machine had a unique set of particles selected from the distribution described below. This configuration of fast workstations allowed us to simulate a very large number of particles in a relatively short period of time (total run time was approximately three months for the Jupiter/Saturn zone).

Our code frequently outputs restart files in the eventuality that, should the

simulation be halted for any reason, it can be resumed with a minimal loss of computer resources. Early in the numerical evolution of the system, while most particles were present, output files were produced every simulated 10^3 years. As the system evolved and the number of survivors decimated, the output interval was increased to every 10^6 simulated years.

In order to compare the rounding and other properties of different workstations, one of the restart files, taken immediately after the Runge-Kutta/Richardson initialization, was simultaneously integrated on a Sun SPARC station, a Silicon Graphics station, and a DEC Alpha station. All workstations generated the same final results for a 2,000 test particle run after a 12 million year integration. Although all of the computations presented here were performed on the same Hewlett-Packard workstations, it was reassuring to note that these test runs performed on different workstations, but using the same IEEE arithmetic standards, obtained the same results. It should be mentioned that, although we had a major allocation of resources on a massively parallel CRAY T3D supercomputer, much of the software on this new computer was at the time untested.

One hundred thousand test particles were placed in elliptical and inclined orbits about the Sun. Their trajectories were integrated for up to 1 billion years, or until they were removed from the simulation (as described below). The test particles were treated as massless, and were subject to the gravitational influences of the Jovian planets as well as the Sun. The sun and planets were mutually-interacting. Initial planetary positions and velocities were generated using JPL ephemeris DE 245 (Standish, 1984), and each of the test particle orbital elements were randomly selected according to the following prescription. The test-particle semimajor axes were Gaussian distributed such that the average semimajor axis was equal to the average of Jupiter's and Saturn's, and that, the 3σ points (i.e. three times the standard deviation) of the distribution were coincident with Jupiter's and Saturn's semi-

major axes. Since the region of interest was primarily the zone between Jupiter and Saturn, no initial particle semimajor axes were allowed inside 4.703 AU (Jupiter's semimajor axis minus 0.5 AU), outside 10.039 AU (Saturn's semimajor axis plus 0.5 AU), or within either of those planets' activity spheres (Danby, 1988, p. 267). The initial inclinations were similarly Gaussian distributed with an average of 0° and standard deviation of $100'$. Eccentricities were randomly chosen from 0 to 1 from an exponential distribution with an e-folding constant of 0.1. This means that particles with eccentricities of 0.1 occur with a $1/e$ lower frequency as those with eccentricities of 0.0, and so on. The initial phase angles, longitudes of nodes, and longitudes of perihelia were randomly selected from a uniform distribution between 0 and 2π . Random number generation was performed using procedures (RAN2, EXPDEV, and GASDEN) from Press et al. (1988). Input/output was done in heliocentric coordinates while the integrations were performed in a barycentric frame for all bodies, including the Sun. The latter provided us with an additional accuracy check on the center of mass' position and velocity.

In this simulation, a test particle was considered to be eliminated if it met one of three criteria. Particles were removed from consideration if they underwent a close-encounter and passed within the activity sphere of a planet. Here, we used the modified definition of activity radius from Holman and Wisdom (1993), namely

$$r_{\text{act}} = a_0 \left(\frac{m_p}{M_\odot} \right)^{2/5},$$

where m_p is the mass of a given planet, and a_0 its initial semimajor axis. In contrast, it is noteworthy that G1990 employed a sphere of influence with an $\approx 30\%$ larger radius. A particle was considered ejected from the solar system, and thus removed from the simulation, if (1) it had positive energy relative to the Sun and all of the planets, (2) it had heliocentric radius greater than 50.0 AU, and (3) the projection of its velocity against a radial line from the Sun was positive, i.e. was

on an outbound trajectory with $\vec{r} \cdot \vec{v} > 0$. We included the third ejection criterion because we recognized the possibility, albeit small, that an incoming particle on a hyperbolic (unbound) orbit could, through planetary interactions, lose energy and subsequently rebound (Everhart, 1968). Finally, if a particle came within 1 AU of the Sun, we calculated its perihelion distance. If this was less than R_{Sun} , then the particle was eliminated from the simulation. It should be noted that, throughout the entire 100,000 particle simulation, no such “sun-grazers” (Levison and Duncan, 1994) were detected, despite the additional mass of the inner planets being added to that of the Sun.

This concludes our description of the numerical methods employed in this investigation. A more detailed and comprehensive description will be found elsewhere. We now direct our attention to the results of these investigations of the Jupiter/Saturn zone.

4. RESULTS

As is often the case when exploring a new problem (or an old one using refined tools), the initial phase of our data analysis was exploratory— to try to identify the different periods of evolution and the relevant physics. The physical ingredient that we believe must be central to this problem is kinetic theory, as appropriate to self-gravitating systems, but other processes could conceivably be important. In Fig. 5, we plot the number of surviving planetesimals as a function of time and observe that there are three basic evolutionary periods in this problem. First, there is a transient phase associated with the start of the simulation where many planetesimals are quickly eliminated by either the activity spheres of Jupiter and Saturn, or by virtue of being on very eccentric, even planet-crossing, orbits from the beginning. Second, there is a gravitational relaxation phase where the surviving particles undergo a random walk in momentum space, being scattered successively by gravitational encounters from the planets until they are eliminated after interacting with an

activity sphere. (If we had displayed the results in log-linear fashion, we would see an essentially exponential decay during this phase where the e-folding time evolves upward as the winnowing proceeds.) Finally, there is a phase characterized by long-lived particles that reside either in the neighborhood of stable Lagrangian points or, albeit less often, in candidate stable niches (near commensurabilities), or, in elongated orbits with very long periods. We have obtained estimates of the e-folding time scales appropriate using a nonlinear exponential fit to the different time ranges. During the first phase, extending from the time origin to 3×10^3 yr, the e-folding time was observed to be $\approx 6.8 \times 10^3$ yr. During the gravitational relaxation phase, from 10^5 to 5×10^5 yr, the e-folding time was observed to be $\approx 2.0 \times 10^5$ yr. Finally, during the “Lagrangian niche” phase, from 10^7 yr to 10^{11} yr, the e-folding time has become extremely long, of order 2×10^8 yr.

In Fig. 6, we provide an illustration that describes how this situation unfolds. We show a Gaussian, signifying the planetesimal swarm’s initial distribution in semi-major axis, flanked by the activity spheres of Jupiter and Saturn. With the initiation of the simulation, many of the planetesimals will have trajectories that quickly bring them into the path swept up by the activity spheres of Jupiter and Saturn. Previously, FLS89 had noted that there was a 2% to 6% difference between the time a particle’s orbit became planet crossing and entry into a close approach. It is appropriate to describe this initiation phase as a collision of “hard spheres” with the point planetesimal particles. This aspect of kinetic theory was first developed by Chapman and Enskog and is clearly described in the text by Chapman and Cowling (1971): the collision frequency ν varies as $n\sigma\Delta v$ where n is the number density of colliders (i.e. Jupiter and Saturn), σ is the “collision cross section” of the collider, namely πR^2 where R is the radius ≈ 0.34 AU of the two activity spheres, and Δv is a measure of the velocity difference between planetesimal and planet. The number density is estimated from the volume appropriate to our initial

planctesimal distribution (see above) and has the form of a torus extending between the orbits of Jupiter and Saturn, and subtending an angle normal to the invariable plane with respect to the sun of $\approx 20^\circ$. We took the corresponding volume to be $\approx 516 \text{ AU}^3$. Since the circular velocity $v \propto a^{-1/2}$, we estimated the differential velocity Δv according to the velocity difference between a planet at the center of an activity sphere and a planetesimal at its periphery, hence $\Delta v \approx (\Delta a/2a)v$. For Jupiter, we obtained $\Delta v \approx 2.3 \times 10^{-4} \text{ AU/Dy}$ (with a slightly smaller value for Saturn). Putting these quantities together yields an approximate time scale, i.e. the reciprocal of ν , of $8.2 \times 10^3 \text{ yr}$, in close agreement with our fit to the data shown in Fig. 5.

The important point illustrated by Fig. 6 relates to the gravitationally-dominated phase of evolution when planetesimals undergo a form of random walk in momentum space, undergoing intermittent gravitational boosts as they wend their way among the Jovian planets. There is a time scale associated with this process which describes the length of time required for a particle to undergo a major deflection by a planet. The process of gravitational relaxation was first developed by Chandrasekhar (1943) and was elaborated upon in a major way for general Coulomb interactions by Spitzer (1962). For more up-to-date treatments including significant improvements in the treatment of gravitational interactions in a planetesimal swarm in the context of solar system dynamics, see Stewart and Kaula (1980) and Stewart and Wetherill (1988).

Figure 6 reminds us that Δv is greatest at the center of the Gaussian distribution and diminishes as the particle draws near to a Jovian planet. We can employ the Virial Theorem to relate Δv to the effective interaction distance r between a planetesimal and a planet of mass M , namely $GM/r \approx \Delta v^2$. Accordingly, we replace the "hard sphere" cross section σ introduced above by the velocity dependent version $\sigma_{\Delta v}$ according to $\pi r^2 \approx \pi (GM/\Delta v^2)^2$. Then, the appropriate time scale

τ varies as $\Delta v^3 / \pi n(GM)^2$. This expression shows us that gravitational collision times are smallest when Δv is smallest. Hence, planetesimals which closely flank the activity spheres are among the first to be deflected into the path of these spheres of influence. Planetesimal material closer to the center of the Gaussian distribution in Fig. 6 require much more time to complete their random walk into the path of a moving activity sphere. The time scale appropriate to the minimum relevant Δv is, in fact, approximately the same as that we derived for the activity sphere. (That should be no surprise since the activity spheres describe a form of force or virial balance.) What is more instructive is to estimate the lifetime of those particles which must undergo the greatest change in Δv . As we will see later, the scattering influence of Jupiter on planetesimals drives many nearby planetesimals out to the sphere of influence of Saturn. (A smaller number of particles are shepherded from Saturn into the path of Jupiter's activity sphere.) For these longest-lived particles, Δv is simply the differential velocity between the orbits of Jupiter and Saturn, or about 2.6×10^{-3} AU/Dy. Since we wish to consider gravitational scattering by either Jupiter or Saturn, we will employ the geometric mean of their GM values, or 1.55×10^{-7} AU³/Dy². We obtain, therefore, a gravitational relaxation time scale 1.7×10^5 yr, in close agreement with our empirical value of 2.0×10^5 yr. 'But, a simple kinetic theory and ideas from the statistical mechanics of particulate systems and the Coulomb force permits us to theoretically derive some of the basic features of our simulations! It is important to note that the evolution of the solar system on time scales long compared to 1 (F') yr leads to effects, such as resonance, not describable by simple kinetic theory.

One final set of comments is in order regarding the *relative* rates of planetesimal deflection by the major planets. Geometric and dynamic intuition would imply that planetesimals on highly inclined orbits will be less likely to deviate from their respective courses than planetesimals traveling in the plane—the odds for mutual

avoidance become much greater for planetesimals with highly inclined trajectories; also, it is more difficult to change the direction of the angular momentum vector than its magnitude. Another element of geometric intuition emerges when we consider the relative importance of planetesimal deflection by Jupiter or by Saturn. The relative number of planetesimals swept away by the activity spheres of Jupiter and Saturn (which have essentially the same radius) should vary as the ratio of the areas of the two annuli swept out by these two Jovian planets, a ratio of approximately 1.0:1.9 (this presupposes a "symmetric" initial distribution between them. This is an additional feature we should look for in our simulation). Lastly, our discussion of kinetic theory has ignored the roles of Uranus and Neptune, which have a relatively modest influence on planetesimal evolution. Basically, the outer Jovian planets can tilt only those planetesimals whose semimajor axes and/or eccentricities have been pumped up so as to come within their range of influence. Thus, although Uranus and Neptune have a small but significant role, elementary kinetic theory is inadequate to predicting the singular gravitational events that can propel planetesimals into their spheres of influence.

In previous work, investigators showed plots of the lifetimes of all particles in their survey, over the semimajor axis range of interest subdivided into smaller intervals. This is no longer practical when you have samples which range from 10^4 to 10^5 particles. To display this information we have chosen two formats. Fig. 7 shows the minimum and maximum lifetimes of particles in our simulation as a function of their initial semimajor axis range in 0.1 AU semimajor axis intervals. Note the features from 5.0 to 5.3 AU, and from 9.3 to 9.6 AU. These correspond to particles librating in Trojan, "horseshoe", or "tad pole" orbits with respect to Jupiter and Saturn, respectively. Only 65 particles of the original 105 survived the first 100 million years integration. Of these, 57 were in Trojan orbits, 7 were co-orbiting with Saturn, and one was situated at 6.6 AU. All particles which ended the

simulation in Trojan orbits began their lives there, and did not arrive at these niches as a result of dynamical evolution. The same is true of the Saturn co-orbiters. The Jupiter and Saturn co-orbiters were removed from the simulation at 100 My, but the particle at 6.6 AU survived the integration with its semimajor axis virtually unchanged for one billion years maintaining its small eccentricity (≤ 0.075) and inclination ($< 0.35^\circ$).

The plot of maximum and minimum lifetimes in Fig. 7 contains only limited information. The maximum lifetimes often represent the duration the simulation in contrast with the time spent in the Jupiter/Saturn zone. As an example, one particle with an initial semimajor axis of 7.9 AU achieved a semimajor axis of 109,000 AU (corresponding to a period of approximately 3.6×10^7 years) but nevertheless remained bound to the solar system. On its next passage through the solar system, its orbit was perturbed and it was subsequently classified as ejected. The fact that this lone particle survived so long in the simulation before meeting our criteria for elimination is another indication that the maximum lifetimes can be misleading. Similarly, the minimum-lifetime particles for each range were relatively eccentric and often were on planet-crossing orbits from the onset of the simulation. In short, maximum and minimum value statistics can be misleading.

A much more informative measure of the expected lifetimes of particles in the Jupiter/Saturn zone is shown in Fig. 8. Here we considered the lifetime distribution in each semimajor axis interval and identified the first and third interquartile ranges, namely the times below which 25% and 75%, respectively, of the planetesimals had been eliminated. (Another measure of statistical variability could have been produced by plotting the mean lifetime with "error bars" denoting one standard deviation.) Again, we see strong features at 5.2 and 5.3 AU corresponding to Trojan orbits, but the analogous features for Saturn co-orbiters have sharply decreased in magnitude. Also note the depression at 7.3 AU, corresponding to the Saturn 3:2

mean motion resonance and the Jupiter 3:5 resonance.

Although it was one particle out of 100,000, we were curious about the conditions under which the particle at 6.6 AU remained stable and relatively unchanged throughout the entire 10^9 year integration. We therefore performed a 2,000-particle targeted search of the region surrounding it. All distributions of orbital elements were the same as described earlier, with the exception of semimajor axis which was uniformly distributed between 6.4 and 6.8 AU. No particle in this subsequent search survived more than 2.6 million years. We plan to return to the question of the stability of this and nearby orbits in the future.

Table 2 provides an indication of the relative significance of various mechanisms for depleting planetesimals from different semimajor axis ranges. In each 0.1 AU interval we indicate how many particles presently remain, how many were eliminated by the activity spheres of Jupiter, Saturn, Uranus, and Neptune, respectively, and how many were ejected from the solar system. (Importantly, no planetesimals were eliminated by the "sun grazing" criteria.) Here, direct comparisons with the results of other researchers are difficult because (1) our simulation was not confined to the invariable plane as were most of the others (with the exception of GD90 who examined orbits at 10°), (2) our simulation was not limited solely to Keplerian Jovian planetary orbit S_1 , and (3) the much smaller number of particles employed in previous surveys renders such counts more susceptible to the "statistics of small numbers" (Newman et al., 1992). Importantly, we note that we can make statistically valid inferences about the significance of various mechanisms, since the relative uncertainty in our results varies as $O(N^{-1/2})$.

Uranus and Neptune together eliminate about 1/2% of the planetesimals. Surprisingly, no planetesimals are lost by being directly transported into the region occupied by the terrestrial planets. Of our 105 planetesimals, only 48 were ejected from the solar system. HW93, however, observed "no non-elliptic orbits were de-

ected) ("close encounter." It is entirely possible that this is an outcome of the relatively small sample size which they employed.

Saturn is the planet colliding with most of the lost planetesimals, but usually it is Jupiter that perturbs them into its path, as found by WKN90. We show this in the half-tone Figs. 9 and 10. Recall that our initial particle distribution is an annulus centered half way between Jupiter and Saturn and diminishing as a Gaussian away from the midpoint. Were we to produce from our original distribution of 10^5 planetesimals a grey scale representation of the density of points as a function of position (with darker implying denser), we would obtain a very smooth toroidal shape with gently varying shading. What, we have chosen to do in Figs. 9 and 10 is to represent the *relative* number of planetesimals—varying from 0 to 1—that were ultimately removed by the activity spheres of Jupiter and Saturn, respectively.

These two figures share two prominent features. First, they show the subtle imprint of what is likely a fractal geometry or "fractal basin boundaries"—see Ott (1993) in the ultimate fates of the planetesimal swarm. This is an indicator of the presence of Hamiltonian chaos in our planetesimal population and makes very clear how sensitive behavior near separatrices are to the starting positions (i.e. phase angles) of the test particles. Second, they show the importance of scattering as a mechanism in delivering planetesimals from the annular neighborhood of one planet to the sphere of influence of another. Given the intensity of the grey scale in Fig. 9, we see that Jupiter gravitationally scatters the bulk of the planetesimal population into the path of Saturn's activity sphere. In Fig. 10, we see that Saturn has a similar, albeit smaller, role in propelling planetesimals inward and into the path of Jupiter's sphere. (G1990 note that "crossing a planet's orbit will not necessarily mean that the first close planetary approach will occur with *that* planet." FLS89 also noted that an orbit which crosses Saturn's can very quickly evolve into one that crosses Jupiter's. These figures are unmistakable evidence of both.) Indeed,

these two figures demonstrate the complexity contained within the dynamics, and provides a compelling reason for using only the most accurate integration techniques available for studying the stability of solar system niches.

We now want to visualize the demographics of the planetesimals which are eliminated as a function of time. To do this, we plot in Fig. 11 over successive 100 Jupiter orbit time intervals the mean and one standard deviation of the semimajor axis distribution deflected during each 100 orbit time window. (Specifically, we show the mean \pm 1 standard deviation as a bar in each interval of time.) We observe that those particles whose semimajor axes reside near the orbits of Jupiter and Saturn are among the first to be eliminated. The average semimajor axis remains nearly constant at 7.3 AU, while the extent of one standard deviation steadily decreases. Ultimately, the number of planetesimals eliminated in each time window is too small to yield statistically valid conclusions. Nevertheless, we observe the unmistakable trend of winnowing of planetesimals from the vicinity of Jupiter and Saturn into the heart of the Jupiter/Saturn zone. This observation agrees with the kinetic theory prediction derived earlier in the context of Fig. 6.

Earlier, we discussed the role of inclination from a simple geometric standpoint, expecting to find that subpopulations of planetesimals with more inclined trajectories would experience reduced rates of elimination. In Table 3, we consider according to their initial distribution our set of 10^5 planetesimals grouped in 1° inclination intervals and display the numbers removed by the various available mechanisms. These "mechanisms" include, as in Table 2, the four Jovian planets and solar system ejection, as well as show what number of planetesimals survived 10^8 years. What is particularly noteworthy is the relative effectiveness of Saturn's activity sphere eliminating planetesimals in contrast with Jupiter's. We reported earlier the expectation, from the geometry the annuli swept out and kinetic theory, that Saturn would appear to be 1.9 times more effective at eliminating planetes-

imals than Jupiter. The column in Table 3 denoted "S:J Ratio" shows that this proportion remains near 1.9, never descending to 1.0. (We do not display this ratio, although it remains consistent with our prediction, when the total planetesimal count in a given inclination region drops below 1,000 as it would become overly sensitive to the small population.)

In contrast, GD90 reported that particles with nonzero inclinations began to be removed *later* in the simulation than those in the invariable plane, but that once planetesimal removal began in the plane it would proceed at a faster pace. After approximately 20,000 years, GD90 claimed that the fraction of remaining particles was the same independent of initial inclination. Fig. 12 shows a family of curves displaying the relative depopulation of the planetesimal swarm as a function of initial inclination starting at 0° and varying in 5° increments up to 20° . We see major differences between our results and those of GD90 in the comparative depletion rates for the 0° and 10° curves. To better understand this difference, we considered a subset of our population of planetesimals whose semimajor axes ranged from 6.76 AU to 8.06 AU, the same initial range employed in GD90. Fig. 13 shows the comparative depletion rates and we observe an *order of magnitude* difference in the relative depletion rate. The half-life of the 0° inclination particles in Fig. 13 is observed to be 3×10^3 yr while the 10° planetesimals have a half-life of 104 yr. These numbers should be compared with our initiation phase depletion time scale of 6.8×10^3 yr and our kinetic theory calculation of 8.2×10^3 yr. The GD90 time scales are too long by an order of magnitude. This is particularly surprising since they employed activity spheres that were 30% larger than we had. A larger sphere of influence cross section, as we noted earlier, can be expected to give a *shorter* lifetime.

In comparing relative removal mechanisms, GD90 noted that for particles in the plane, close approaches with Saturn were more numerous than those with Jupiter

by a ratio of $2(6/175 \approx 1.520)$, while for the inclined population, the roles were reversed and close approaches with Jupiter occurred $223/182 \approx 1.226$ times more frequently—we give their observed populations as a possible indication of the role of small $(1/175)$'s. The reason for this reversal in roles, they claimed, was that “inclined particles are typically further from the plane near Saturn than near Jupiter and therefore less likely to have encounters.” While true, the particles must eventually pass through the plane.

We showed in our Table 3, that particles of all inclinations tended to have more frequent close approaches with Saturn. Our results differ from those of the less precise GD90 survey in a fundamental way with respect to time scales and the relative importance of different mechanisms. Could this then be evidence that symplectic integration schemes that employ large time steps can give, without warning, qualitatively incorrect results in problems with subtle separatrix geometry? Evidence supporting this conclusion comes from Sanz-Serna and Calvo (1994) who explored a variety of symplectic integrators in solving the Henon-Heiles problem. They tested six integrators, including one by Candy and Rozmus (1990) which was used in GD90, as a function of step size. Sanz-Serna and Calvo showed that, until the step size dropped below some value (which they proceeded to determine), the integrator would give qualitatively incorrect results when employed in chaotic regimes. This result is particularly important given the cost of contemporary integrations and the efforts employed by many investigators to minimize them. The lesson to be learned is that *any* integrator, symplectic ones included, can give misleading results unless extraordinary care is taken while on the edge of chaos.

In Fig. 14, we plot the mean eccentricities and “error bars” (as in Fig. 11, corresponding to 1 standard deviation) of the planetesimals which are eliminated over successive 100 Jupiter orbit time intervals. The essential feature here is that, as time proceeds, the mean eccentricities and their variances diminish, indicating that

highly eccentric particles are the first to disappear and we are left with a population of particles with ever-decreasing eccentricities.

Analogous to Fig. 11, Fig. 15 provides a family of curves that show removal rates as a function of eccentricity. We observe that more eccentric orbits have markedly shorter lifetimes than less eccentric ones, as we would intuitively expect. FL89 suggested that more eccentric particles could be somewhat more stable if their eccentricity approximated that of the perturbers. Looking at the removal curve for $c = 0.05$ (where, for Jupiter, $e = 0.048$ and, for Saturn, $e = 0.056$) we see no indication of this.

Tables 4 and 5 describe an outward migration of planetesimals in the simulation—a feature alluded to in Figs. 9 and 10, as well as Table 2. Table 4 shows the final semimajor axis range for all 100,000 particles at the end of 100 My simulation time. Over 11% of the particles had their final semimajor axes outside of that of Saturn at the end of the simulation, 48 were completely ejected from the solar system. Less than 2% of the particles were injected into the inner solar system. Even within the Jupiter/Saturn zone, the trend was for the particles to move outwards—this can be seen in Table 5. Table 5 shows the initial and final semimajor axes (and standard deviations) for the sample of particles eliminated by collision with the activity sphere of each planet. The average semimajor axes of the particles killed by every planet indicate that the trend was for the particles to migrate outwards, with their orbits becoming increasingly eccentric in the process. Even particles eliminated by Jupiter had, on average, semimajor axes greater than that with which they began the simulation.

The dynamical effects governing mixed populations of “heavy” and “light” self-gravitating particles over very long periods of time have been a subject of investigation, especially in galactic dynamics, for many years. Overwhelming evidence has emerged that a “mass segregation effect” occurs where the heavy particles shed en-

ergy and angular momentum, thereby gravitating inwards, while the lighter particles gain both energy and angular momentum causing them to move outwards (Farouki and Salpeter, 1982; Farouki et al. 1983; Spitzer, 1987; Stewart and Wetherill, 1988), sometimes being ejected from the system. This mass segregation phenomenon became widely used as an empirical diagnostic for the reliability of N -body galactic dynamics codes.

We believe that Tables 2, 4, and 5, as well as Figs. 9 and 10 indicate that our system exhibited this phenomenon.

Finally, in Fig. 16, we plot the final positions of the Sun, Jupiter, Saturn, and all surviving planetesimals, projected onto the invariable plane after 100 My simulation time. What we observe is a simulated Jupiter/Saturn zone which looks very much like the actual. Because the solar system has provided us with 4.6 billion years of empirical evidence to indicate that the Jupiter co-orbiters (Trojans) are stable, and because the work of de la Barre et al. (1996) has indicated that Saturn co-orbiters (Bruins) may be similarly stable over billion-year time periods, we integrated only the "outlier" at 6.6 AU from 100 My to 1 Gy.

5. CONCLUSIONS

This concludes our investigation of the Jupiter/Saturn zone; the Saturn/Uranus and Uranus/Neptune zones are the subject of a sequel. (The Trans-Neptune zone and the dynamics of Pluto are a more distant objective.) Our investigation has employed the most accurate numerical techniques ever brought to bear on this class of problems and employing nearly 10^3 times as many test particles than any previous study. The statistics we have obtained are robust, and we can derive many of the relevant quantitative results using kinetic theory.

The outcome of this study that is relevant to our solar system's origin is that niches for planetesimal material will be few and far between. The Lagrange points—the Trojans of Jupiter and the Bruins of Saturn (de la Barre et al. 1996), possibly

some highly inclined and/or eccentric (i. e. Hilda group) orbits, plus conceivably a few nearly commensurable regions in the Jupiter/Saturn zones will remain stable over a significant fraction of the age of the solar system. For the bulk of this material, it appears that we are seeing evidence for an evolutionary process, where early solar system material, on the edge of chaos (Newman et al., 1995) and exposed to qualitative bifurcations in their dynamics, was removed from almost, all regions in the Jupiter/Saturn zone. The outcome of this study relevant, to our solar system's dynamics is that the primordial planetesimal swarm has resided in a phase space divided into regimes by separatrices which define their trajectories and fate. In order to capture even the "statistical" character of the solar system's planetesimal evolution, there is no simple alternative to pushing the frontiers of computation to the complete accuracy available with today's advanced computers.

Acknowledgments: The authors would like to thank John W. Dunbar of Hughes Aircraft Corporation, Norman Field, and Robert E. Bell for their computational assistance. We would also like to thank E. Myles Standish and Hester A. Neilan of the Jet Propulsion Laboratory, and Merton E. Davies of the RAND Corporation for their assistance with ephemerides and other helpful discussions. We are particularly grateful to Ferenc Varadi for many discussions. This research was supported in part by NASA grant NAGW 3132 and by an INCOR grant from Los Alamos National Laboratory.

REFERENCES

- Aarseth, S..1. 1972. Direct integration methods of the N-Body problem. In *Gravitational N-Body Problems, IAU Colloquium No. 10* (M. Lecar, ed.) pp. 29-43. (Dordrecht: Reidel).
- Ahmad, A., and L. Cohen 1973. A numerical integration scheme for the N-body gravitational problem. *J. Comput. Phys.* **12**, 389-402.
- Applegate, J.H., M.R. Douglas, Y. Gürsel, G.J. Sussman, and J. Wisdom 1986. The Outer Solar System for 200 Million Years, *Astron. J.* **92**, 176-194.
- Bate, R.L., D. Mueller, and J.F. White 1971, *Fundamentals of Astrodynamics* (New York: Dover).

- Bell, R.E., K.R. Grazier, W.J. Newman, W.M. Kaula, and J.M. Hyman, 1994. Long Term Integrations of the Solar System: Simplicity Beats Symplecticity, 24th DDA meeting Kingsville, TX. *B. A. A. S.* 26, 1023.
- Bowell, E.L.G. 1996. The Asteroid Orbital Element Database, <ftp://lowell.edu/pub/clgb/astorb.html> (28 October 1996).
- Candy, J., and W. Ozorio 1990. A Symplectic Integration Algorithm for Separable Hamiltonian Functions. *J. Comput. Phys.* 92, 230-256.
- Chandrasekhar, S. 1942. Stochastic Problems in Physics and Astronomy, *Rev. Mod. Phys.* 15, 189.
- Chandrasekhar, S. 1943. *Principles of Stellar Dynamics* (Chicago: University of Chicago Press).
- Chapman, S. and T.G. Cowling 1970. *The Mathematical Theory of Non-Uniform Gases*. Third Edition (Cambridge: Cambridge University Press).
- Cohen, C.J., and E.C. Hubbard 1965. Libration of the Close Approaches of Pluto to Neptune. *Astron. J.* 70, 1013.
- Cohen, C.J., E.C. Hubbard, and C. Oesterwinter 1973. *Astron. Papers Amer. Ephemeris.* 22.
- Cowell, P.H. and A.C.D. Crommelin 1910. "Investigations of the Motion of Halley's Comet from 1759 to 1910," *Greenwich Observations for 1909*, Edinburgh.
- Darby, J. M.A. 1983. *Fundamentals of Celestial Mechanics* (Richmond, Virginia: Willmann-Bell).
- [DiJaBarre, C., M., W.M. Kaula, and F. Varadi] 1996. A Study of Orbits near Saturn's Triangular Lagrangian Points. *Icarus*, 121, 88-113.
- Duncan, M., T. Quinn, and S. Tremaine 1989. The Long-Term Evolution of Orbits in the Solar System: A Mapping Approach, *Icarus* 82, 402-418.
- Everhart, E. 1968. Change in Total Energy of Comets Passing through the Solar System. *Astron. J.* 73, 1039-1052.
- Everhart, E. 1973. Horseshoe and Trojan Orbits Associated with Jupiter and Saturn. *Astron. J.* 78.316-328.
- Farouki, R.T., and E.E. Salpeter 1983. Mass Segregation, Relaxation, and the Coulomb Logarithm in N-body Systems. *Ap. J.*, 253, 512-519.
- Farouki, R.T., G.L. Hoffman, and E.E. Salpeter 1983. The Collapse and Violent Relaxation of N-Body Systems: Mass Segregation and the Secondary Maximum. *Ap. J.*, 271, 11-21.
- Feng, K. and Qin, M. Z. 1987. "The Symplectic Methods for the Computation of Hamiltonian Equations," *Proc. Conf. Num. Methods for PDE's, I-37*, Berlin: Springer-Verlag.
- Feng, K. and Qin, M. Z. 1995. "The Step-Transition Operators for Multistep Methods of ODE's." *Feng Kang's Collected Works, Volume II*, Available at <http://1sec.cc.ac.cn/home1/pub/FENGKang/fkp.html>.
- Franklin, F., M. Lecar, and P. Soper 1989. Original Distribution of the Asteroids II. Do Stable Orbits Exist Between Jupiter and Saturn?, *Icarus* 79, 223-227.
- Giorgini, J.D., D.K. Yeomans, A.B. Chamberlin, P.W. Chodas, R.A. Jacobsen, M.S. Keesey, J. L. Lieske, S.J. Ostro, E.M. Standish, and R.N. Wimberly, 1996. JPL's On-Line Solar System Data Service, to appear in *B. A. A. S.*
- Gladman, B. and M. Duncan 1990. On the Fates of Minor Bodies in the Outer Solar System. *Astron. J.* 100, 1680-1693.

- Goldstein, H. 1996. Ph.D. Dissertation, The Near-O(1)-Limit of Störmer Methods for Long Time Integrations of $y'' = g(y)$. Department of Mathematics, University of California, Los Angeles.
- Grazier, K. R., W.L. Newman, W.M. Kaula, F. Varadi, and J.M. Hyman 1995. An Exhaustive Search for Stable Orbits in the Outer Solar System, 25th DDA meeting, Yosemite, CA-*B. A. A. S.* 27, 1204.
- Grazier, K.R., W.L. Newman, F. Varadi, D.J. Goldstein, and W.M. Kaula 1996. Integrators for Long-Term Solar System Dynamical Simulations, 26th DDA meeting, Washington, DC. To appear in *B. A. A. S.*.
- Haberkorn, M., W.L. Newman, and J.M. Hyman 1996. Life on the Edge of Chaos: Symplectic Integration over Long Times, 26th DDA meeting, Washington, DC. To appear in *B. A. A. S.*.
- Hairer, E., S.P. Norsett, and G. Wanner 1991. *Solving Ordinary Differential Equations I: Nonstiff Problems*. Second Revised Edition (Berlin: Springer-Verlag).
- Henrici, P. 1962. *Discrete Variable Methods in Ordinary Differential Equations* (New York: John Wiley & Sons).
- Higham, N.J. 1993. The Accuracy of Floating Point Summation, *SIAM J. Sci. Comput.* 14, 783-99.
- Higham, N.J. 1996. *Accuracy and Stability of Numerical Algorithms* (Philadelphia: Society for Industrial and Applied Mathematics).
- Holman, M.J. and J. Wisdom 1993. Dynamical Stability in the Outer Solar System and the Delivery of Short Period Comets. *Astron. J.* 105, 5, 1987-1999.
- Kincaid, D. and W. Cheney 1991. *Numerical Analysis: Mathematics of Scientific Computing* (Pacific Grove, CA: Brooks/Cole), 436-442.
- Lecar, M. and F.A. Franklin 1973. On the Original Distribution of the Asteroids 1, *Icarus* 20, 422-436.
- Lessnick, M.K. 1996. Ph.D. Dissertation, Stability Analysis of Symplectic Integration Schemes. Department of Mathematics, University of California, Los Angeles.
- Levison, H.F. and M. J. Duncan 1994. The Long-Term Dynamical Behavior of Short-Period Comets, *Icarus*, 108, 18-36.
- Marsden, B.G. ed. 1996. *Minor Planet Circulars*, Cambridge, MA: Minor Planet Center; also, Marsden, B.G. 1996. *Minor Planet Circulars*. <http://cfa-www.harvard.edu/cfa/ps/mpc.html> (24 October 1996).
- Newman, W.L., M.P. Haynes, and Y. Terzian 1989. Double Galaxy Redshifts and the Statistics of Small Numbers, *Ap. J.* 344, 111-114.
- Newman, W.L., E.Y. Loh, W.M. Kaula, and G.D. Doolen 1990. Numerical Stability and Round-off Properties of Cowell-Störmer Type Integration Methods, *Bull. Amer. Astron. Soc.* 22, 950.
- Newman, W.L., M.P. Haynes, and Y. Terzian 1992. Limitations to the Method of Power Spectrum Analysis: Nonstationarity, Biased Estimators, and Weak Convergence to Normality, E.D. Feigelson and G.J. Babu, eds., *Statistical Challenges in Modern Astronomy* (New York: Springer-Verlag), (137-153, 161-162).
- Newman, W.L., W.M. Kaula, J.M. Hyman, J.C. Scovel, E.N. Loh 1993. Simplicity beats Symplecticity, Paper Presented at the Workshop on Integration Algorithms for Classical Mechanics, Fields Institute for Research in Mathematical Sciences, Waterloo, ON, 13-17 October 1993.

- Newman, W.I., M.P. Haynes, and Y. Terzian 1994. Redshift Data and Statistical Inference. *Astrophys. J.*, **431**, 147-155.
- Newman, W.I., F. Varadi, K.R. Grazier, W.M. Kaula, and J.M. Hyman 1995. Mappings and Integrators on the Edge of Chaos, 25th DDA meeting, Yosemite, CA. *B.A.A.S.* **27**, 1200.
- Newman, W.I., K.R. Grazier, W.M. Kaula, and J.M. Hyman 1996. Simplicity Beats Symplecticity: Multistep Integrators for Second Order Ordinary Differential Equations. in preparation.
- Ott, E. 1993. *Chaos in Dynamical Systems* (New York: Cambridge University Press).
- Press, W.H., B.P. Flannery, S.A. Teukolsky, and W.T. Vetterling 1988. *Numerical Recipes in C: The Art of Scientific Computing* (New York: Cambridge University Press).
- Quinlan, G.D. 1994. Round-Off Error in Long-Term Orbital Integrations Using Multistep Methods. *Celest. Mech. Dyn. Astron.* **58**, 339-351.
- Quinlan, G.D. 1995. personal communication.
- Richardson, L.F. and J.A. Gaunt 1927. The Deferred Approach to the Limit, *Phil. Trans. Roy. Soc. London*, **226A**, 299-361.
- Sanz-Serna, J.M. and M.P. Calvo 1994. *Numerical Hamiltonian Problems* (London: Chapman & Hall).
- Soper, P., F. Franklin, and M. Lecar 1990. Original Distribution of the Asteroids II. Orbits Between Jupiter and Saturn, *Icarus* **87**, 265-284.
- Spitzer, Jr., L. 1962. *Physics of Fully Ionized Gases*, Second Revised Edition (New York: Interscience).
- Spitzer, Jr., L. 1987. *Dynamical evolution of globular clusters*, Princeton: Princeton University Press).
- Standish, E.M. 1994. personal communication.
- Stewart, G.R. and W.M. Kaula 1980. A Gravitational Kinetic Theory for Planetesimals. *Icarus* **44**, 154-171.
- Stewart, G.R. and G.W. Wetherill 1988. Evolution of Planetesimal Velocities, *Icarus* **74**, 542-553.
- Störmer, C. 1907. "Sur les Trajectoires des Corpuscles electrises," *Arch. Sci. Phys. Nat. Geneve.* **24**, 5-18, 113-158, 221-247.
- Weibel, W.M., W.M. Kaula, and W.I. Newman 1990. A Computer Search for Stable Orbits between Jupiter and Saturn, *Icarus* **83**, 382-390.
- Wisdom, J. and M. Holman 1991. Symplectic Maps for the N-Body Problem, *Astron. J.* **102**, 1528-1538.

TABLE CAPTIONS

- Table 1. Previous test particle surveys of the Jupiter/Saturn zone. Shown are the number of particles in the survey, the maximum duration of the simulation, some of the important approximations, and notes germane to the present simulation.
- Table 2. Method of termination in the simulation as a function of initial semimajor axis.
- Table 3. Method of termination in the simulation as a function of initial inclination. We also note the ratio of the number of terminations by Jupiter compared to those of Saturn (until the number of particles in the range drops below 1,000 and we can no longer make statistically meaningful inferences). These values are in relatively good agreement with the ratio 1.9:1 which we derive in the text.
- Table 4. Initial and final mean semimajor axes, as well as standard deviations, for all planetesimals. Particles are grouped according to which planet's activity ultimately was responsible for their removal from the simulation. Note that, in all cases, the mean final semimajor axes are greater than the initial, indicating a general outward migration.
- Table 5. Final semimajor axis ranges for all particles at the time of their removal from the simulation. Approximately 2% of the planetesimals reside in the inner solar system at the time of their termination, while over 1% migrate to the outer solar system, or WCJ beyond.

FIGURE CAPTIONS

- Fig. 1. Absolute RMS longitude error for the 2-D Kepler Problem. Figures are for 16 runs with different initial positions, each having an eccentricity of 0.5. Here and in subsequent figures, R is the correlation coefficient describing the goodness of fit.
- Fig. 2. Relative RMS energy error for 16 runs of the 2-D Kepler Problem.
- Fig. 3. Relative RMS energy error for outer solar system forward/back integration. Values are for times corresponding to 2^4 to 2^{18} orbits of Jupiter. Nonlinear power-law regression reveals a power law index of ≈ 0.46 , indicating the absence of any significant systematic integration error.
- Fig. 4. Absolute RMS longitude error of Jupiter and Saturn for forward/back integrations using 16 different sets of initial conditions.
- Fig. 5. Plot of number of surviving particles in our simulation as a function of time. From this, we can clearly see that the evolution occurs in three phases.
- Fig. 6. An idealized representation of the time evolution of the particles in the Jupiter/Saturn zone. The Gaussian curve represents our initial particle distribution in semimajor axis, whereas the spheres at the wings represent the activity spheres of the two planets. The maximum Δv occurs near the peak of the initial particle distribution. As the wings of the distribution are depleted, they are replenished from inside-out by the planetesimals' random walk in momentum space.
- Fig. 7. Minimum and maximum lifetimes as a function of initial semimajor axis range in 0.1 AU intervals. Spikes at 5.2 and 9.5 AU correspond to Jupiter and Saturn librators.
- Fig. 8. Similar to Fig. 4., particles were grouped according to initial semimajor axis in 0.1 AU intervals and sorted with respect to their lifetimes. High and low values represent the first and third quartiles, respectively. With the exception of the Jupiter and Saturn librators, 75% of the particles are eliminated within 10^5 years, in agreement with previous studies. Jupiter

commensurabilities are indicated across the bottom of the figure, Saturn commensurabilities across the top.

- Fig. 9. Greyscale plot of relative importance (darker more important) of Saturn in eliminating planetesimals. Shading represents the fraction of particles, as a function of initial $X - Y$ position (shown in AU), which enter into Saturn's sphere of influence. (Jupiter and Saturn are located at 5.20 and 9.54 AU, respectively.)
- Fig. 10. Greyscale plot of relative importance (darker more important) of Jupiter in eliminating planetesimals. Shading represents the fraction of particles, as a function of initial $X - Y$ position, which enter into Jupiter's sphere of influence.
- Fig. 11. Average initial semimajor axis ± 1 standard deviation of particles eliminated within each 100 -Jupiter-period range. Note that this average remains remarkably constant with an ever-decreasing standard deviation (that is, until later periods in which we deal with small number statistics). This is consistent with a population that is winnowed from the edge of the distribution inwards.
- Fig. 12. Fraction of remaining particles as a function of time for inclinations of 0, 5, 10, 15, and 20 degrees. Each curve represents particles with initial inclinations which fall within ± 0.5 degrees of the aforementioned values. On short time scales, inclination has a marked effect on lifetimes.
- Fig. 13. Similar to Fig. 9, comparison of depletion curves comparing our results with those of GD90. We see an order-of-magnitude difference in the relative rates of depletion for particles at both 0° and 10° inclinations.
- Fig. 14. Average initial eccentricity ± 1 standard deviation of particles eliminated within each 100 -Jupiter-period interval. Highly eccentric particles are quickly eliminated and we are left with a population characterized by increasingly circular trajectories.
- Fig. 15. Similar to Fig. 9, each curve represents the fraction of particles remaining with initial eccentricities falling within ± 0.005 of 0.025, 0.050, 0.075, 0.100, 0.150, and 0.200. In agreement with Fig. 11, the highly eccentric particles are eliminated more rapidly. This is true even of those with initial eccentricities of 0.05 which, it had been previously suggested, may be longer-lived by virtue of being close in eccentricity to that of their neighboring planets.
- Fig. 16. The positions of the planets, and all surviving particles, at the end of 100 My simulation time, projected onto the invariable plane. What we are left with is a solar system very much like that which we presently observe.

Authors	Number of Particles in J/S Zone	Maximum Integration Duration	Approximations	Notes
Lecar & Franklin (1973)	100	6,000 yr	Jupiter/Saturn only; modeled analytically	Long-lived bands at 6.8 AU and 7.5 AU
Everhart (1973)	221	203,000 yr	Similar model as I.F.73	Long-lived bands at 7.0 AU and 7.5 AU
Franklin, Lecar & Soper (1989)	135	$\approx 10^7$ yr	Jupiter/Saturn only; modeled semi-analytically	Long-lived bands at 7.0 AU and 7.5 AU
Duncan, Quinn & Tremaine (1989)	"Several hundred"	4.5×10^9 yr	Mapping; Jupiter/Saturn on circular orbits	Most orbits planet-crossing in 10^5 yr
Weibel, Kaula & Newman (1990)	125	5.67×10^5 yr	6 th order method; Jupiter & Saturn only; 3-D fully interacting	long-lived bands flank commensurabilities; Stimulus for present work
Soper, Franklin & Lecar (1990)	48	2.4×10^7 yr	Same model as I.F.73	Numerical accuracy check
Gladman & Duncan (1990)	900	2.25×10^7 yr	$e = 0, 0.05, i = 0^\circ, 10^\circ$; 4 th order map;	Inclination had no effect on depopulation time
Holman & Wisdom (1993)	≈ 336	8×10^8 yr	$e = 0$; invariable plane; map; Jovian planets	Majority of particles removed within 10^5 yr
Present Work (1995)	102,000	10^8 yr	Fully 3-D; 13 th order Cowell-Störmer	Most accurate, longitude error $\leq 2^\circ$; reliable statistics & kinetic theory;

Table 1.

Axis	Alive	Jupiter	Saturn	Uranus	Neptune	Eject
4.7	0	9	0	0	0	0
4.8	0	14	1	0	0	0
4.9	0	22	1	0	0	0
5.0	2	20	0	0	0	0
5.1	11	26	1	1	0	0
5.2	34	56	1	0	0	0
5.3	10	94	1	0	0	0
5.4	0	141	4	0	0	0
5.5	0	201	8	0	0	0
5.6	0	308	6	0	0	0
5.7	0	375	20	0	0	0
5.8	0	528	45	0	0	0
5.9	0	744	93	4	0	1
6.0	0	851	1(16	2	1	0
6.1	0	1,083	229	4	2	1
6.2	0	1,255	358	5	1	0
6.3	0	1,444	530	11	0	3
6.4	0	1,554	812	5	4	2
6.5	0	1,667	1,068	16	7	3
6.6	1	1,745	1,501	14	8	0
6.7	0	1,855	1,837	18	3	2
6.8	0	1,916	2,089	8	11	4
6.9	0	2,040	2,431	27	7	2
7.0	0	2,100	2,918	35	7	3
7.1	0	2,164	2,973	34	9	3
7.2	0	2,281	3,155	17	10	4
7.3	0	2,141	3,377	33	7	3
7.4	0	1,816	3,555	33	8	2
7.5	0	1,528	3,791	31	4	2
7.6	0	1,543	3,495	23	11	1
7.7	0	1,326	3,438	24	4	1
7.8	0	1,133	3,392	14	5	3
7.9	0	937	3,102	21	5	4
8.0	0	702	2,892	24	1	0
8.1	0	475	2,647	18	6	1
8.2	0	413	2,364	10	0	1
8.3	0	335	1,989	9	2	0
8.4	0	266	1,677	10	2	0
8.5	0	197	1,336	9	2	1
8.6	0	140	1,048	3	0	0
8.7	0	84	864	4	0	0
8.8	0	55	679	5	0	0
8.9	0	46	507	3	0	1
9.0	0	30	409	3	1	0
9.1	0	12	251	2	0	0
9.2	0	11	192	0	0	0
9.3	0	4	146	2	0	0
9.4	5	6	81	0	0	0
9.5	0	4	59	0	0	0
9.6	2	0	37	0	0	0
9.7	0	4	30	0	0	0
9.8	0	1	13	0	0	0
9.9	0	1	9	0	0	0
10.0	0	0	2	0	0	0
Totals	65	37,703	61,570	482	131	48

Table 2

Inclination	Alive	Jupiter	Saturn	S:J Ratio	Uranus	Neptune	Eject
0 < i < 1	3	2,864	5,107	1.78	24	6	0
1 < i < 2	6	2,798	5,148	1.84	16	5	0
2 < i < 3	5	2,913	4,630	1.59	32	3	1
3 < i < 4	2	3,020	4,496	1.49	4)	10	3
4 < i < 5	7	2,929	4,269	1.46	37	7	3
5 < i < 6	9	2,781	3,990	1.43	44	19	1
6 < i < 7	6	2,552	3,841	1.51	37	10	2
7 < i < 8	3	2,280	3,578	1.57	47	7	3
8 < i < 9	2	2,152	3,412	1.59	26	14	10
9 < i < 10	7	1,877	3,128	1.67	30	11	2
10 < i < 11	4	1,752	2,833	1.62	24	6	3
11 < i < 12	3	1,602	2,609	1.63	25	5	5
12 < i < 13	2	1,237	2,244	1.81	17	6	2
13 < i < 14	0	1,155	2,036	1.76	23	7	5
14 < i < 15	0	980	1,790	1.83	12	5	3
15 < i < 16	0	839	1,634	1.95	12	0	2
16 < i < 17	1	719	1,280	1.78	9	3	1
17 < i < 18	0	644	1,053	1.64	9	1	0
18 < i < 19	5	495	863	1.74	2	2	0
19 < 2 < 20	0	431	712	1.65	1	2	1
20 < 2 < 21	0	329	612	1.86	2	0	1
21 < i < 22	0	272	514		2	1	0
22 < 2 < 23	0	245	427		3	0	0
23 < i < 24	0	202	320		1	0	0
24 < i < 25	0	144	260		0	0	0
25 < i < 26	0	112	217		1	1	0
26 < i < 27	0	103	152		1	0	0
27 < i < 28	0	75	117		0	0	0
28 < i < 29	0	46	67		0	0	0
29 < i < 30	0	40	45		0	0	0
30 < i < 90	0	115	187		0	0	0
Totals	65	37,703	61,571		482	131	48

Table 3

Final Semimajor Axis (by Category)	Number in Range
$a < 4.7$	1,688
$4.7 < a < 10.0:3$	87,068
$10.03 \leq a < 15$	9,804
$15 \leq a < 20$	916
$20 < a < 25$	227
$25 < a < 30$	93
$30 < a < 40$	74
$40 \leq a < 50$	39
$50 \leq a < 60$	12
$60 \leq a < 70$	7
$70 \leq CL < 80$	5
$80 \leq a < 90$	2
$90 \leq a < 100$	3
$100 < a < 200$	4
$200 < a$	10
Ejected	48
Total	100,000*

Table 4

Planet (AU)	Planetary Distance	Planetesimal Mean		Planetesimal Std. Dev.	
		Initial	Final	Initial	Final
Jupiter	5.203	7.028	7.306	0.384	4.790
Saturn	9.539	7.616	8.867	0.353	6.885
Uranus	19.18	7.449	15.567	0.362	5.148
Neptune	30.06	7.300	23.402	0.578	7.7

Table 5

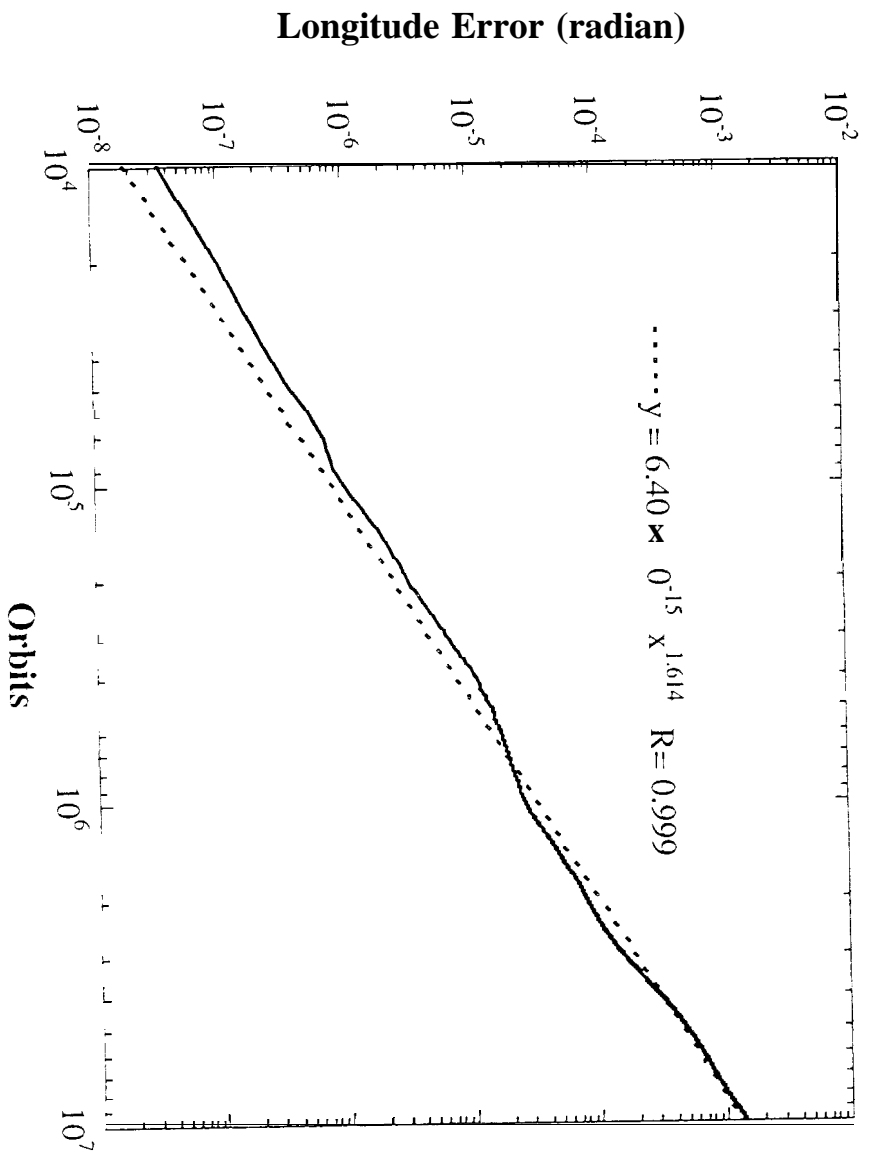


Figure 1

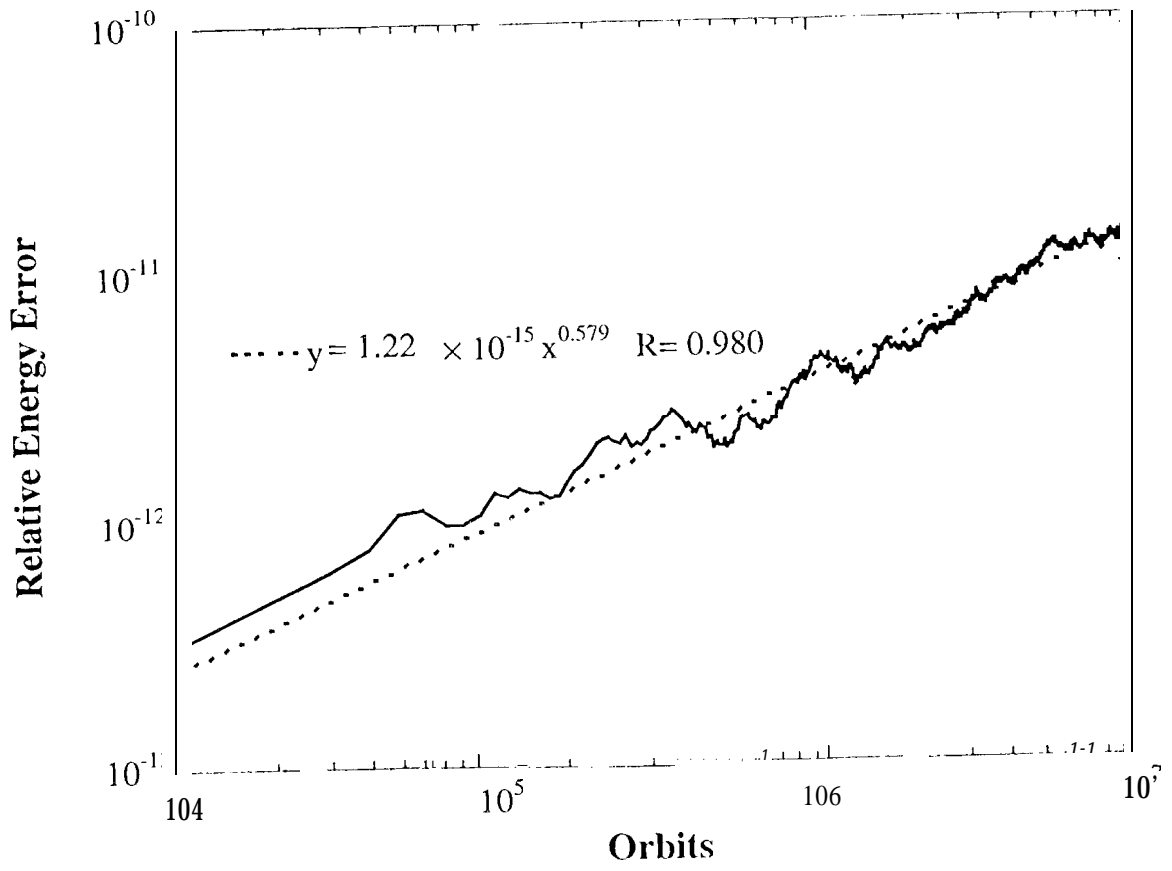


Figure 2

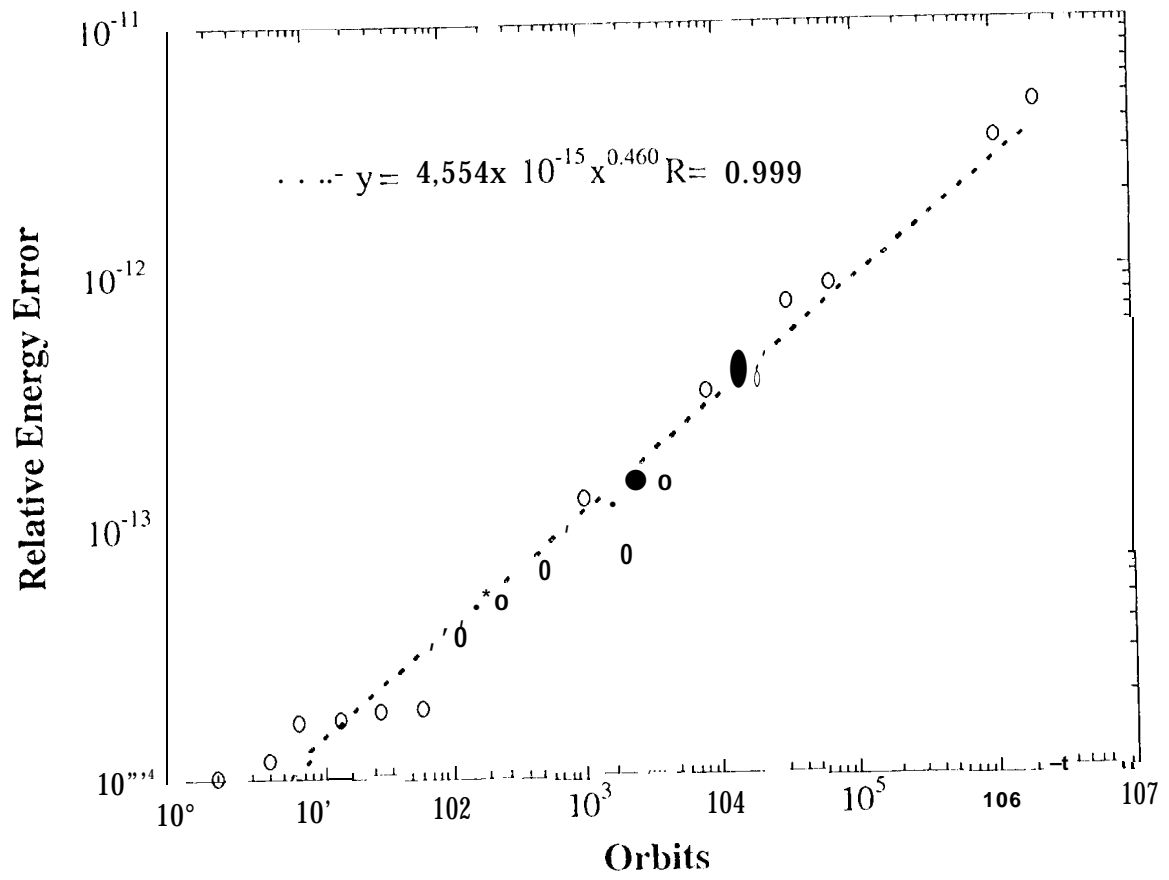


Figure 3

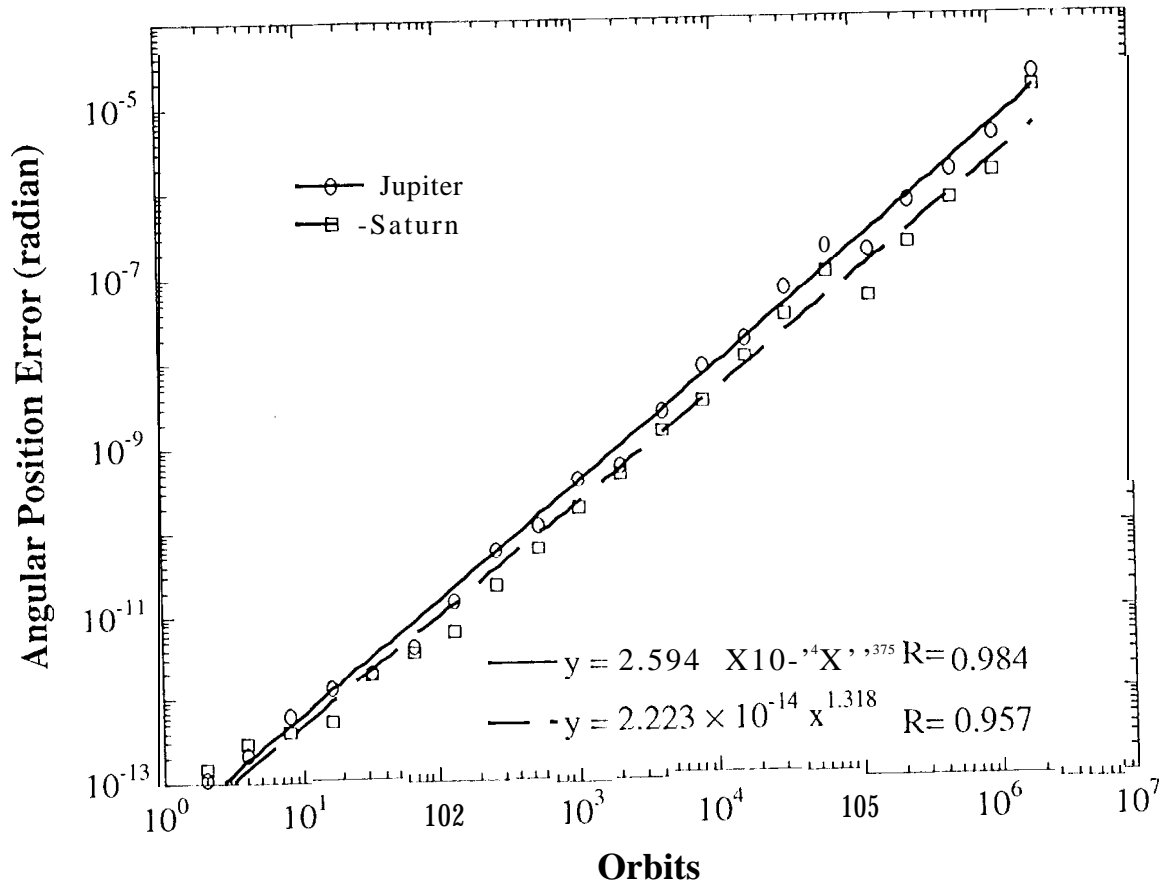


Figure 4.

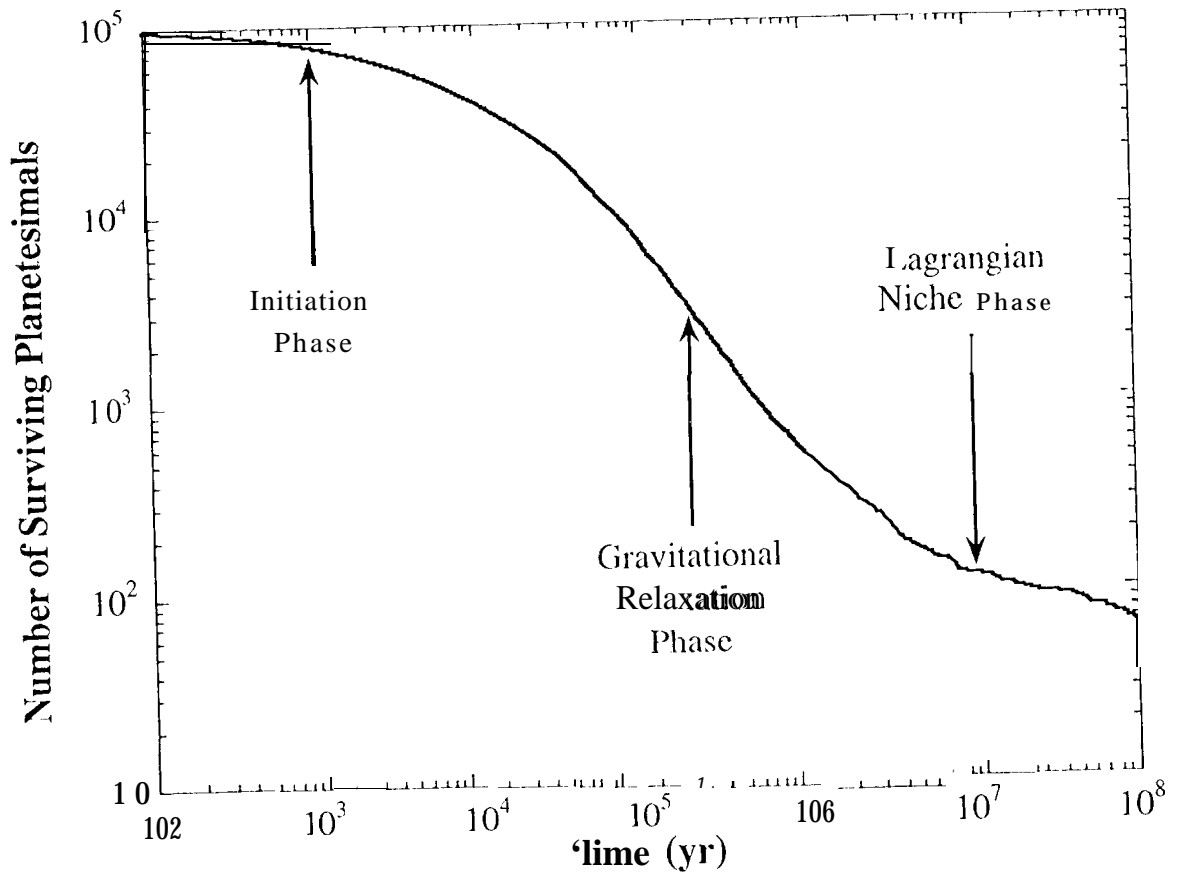


Figure 5

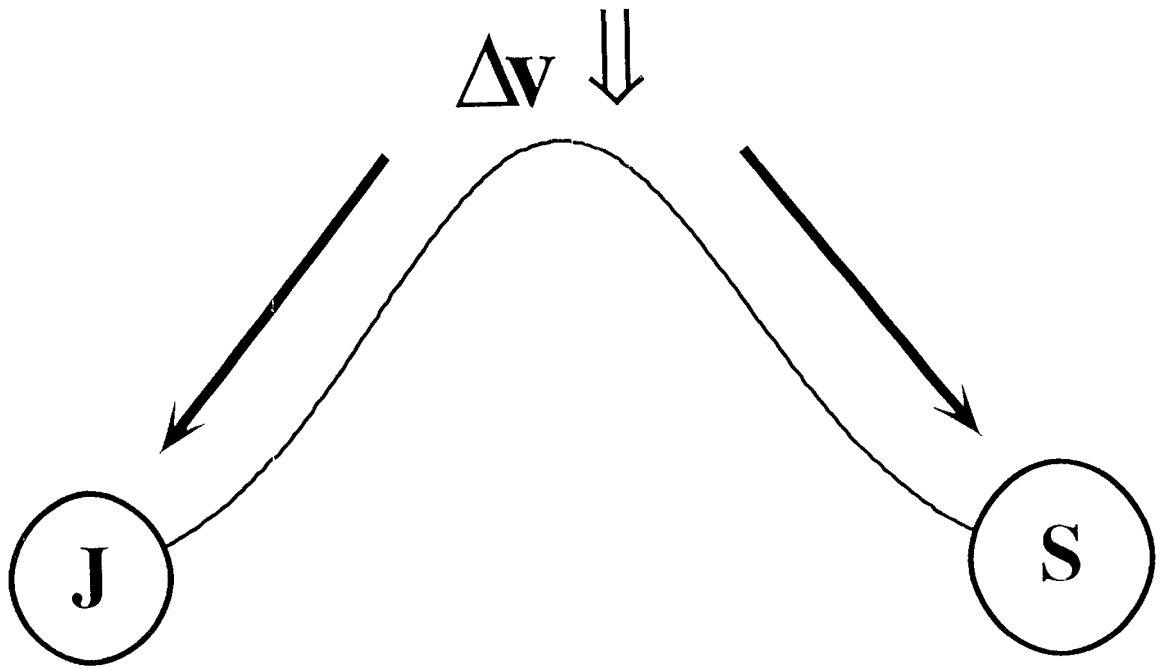


Figure 6

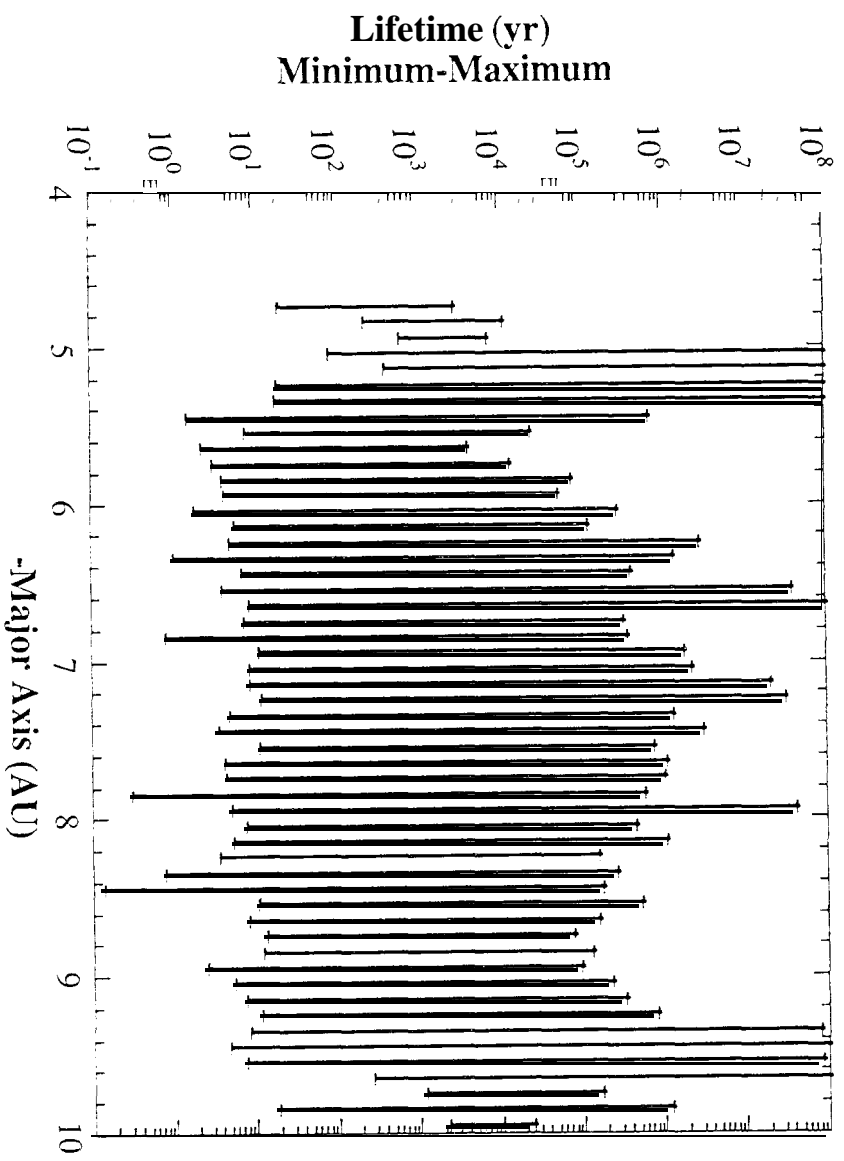


Figure 7

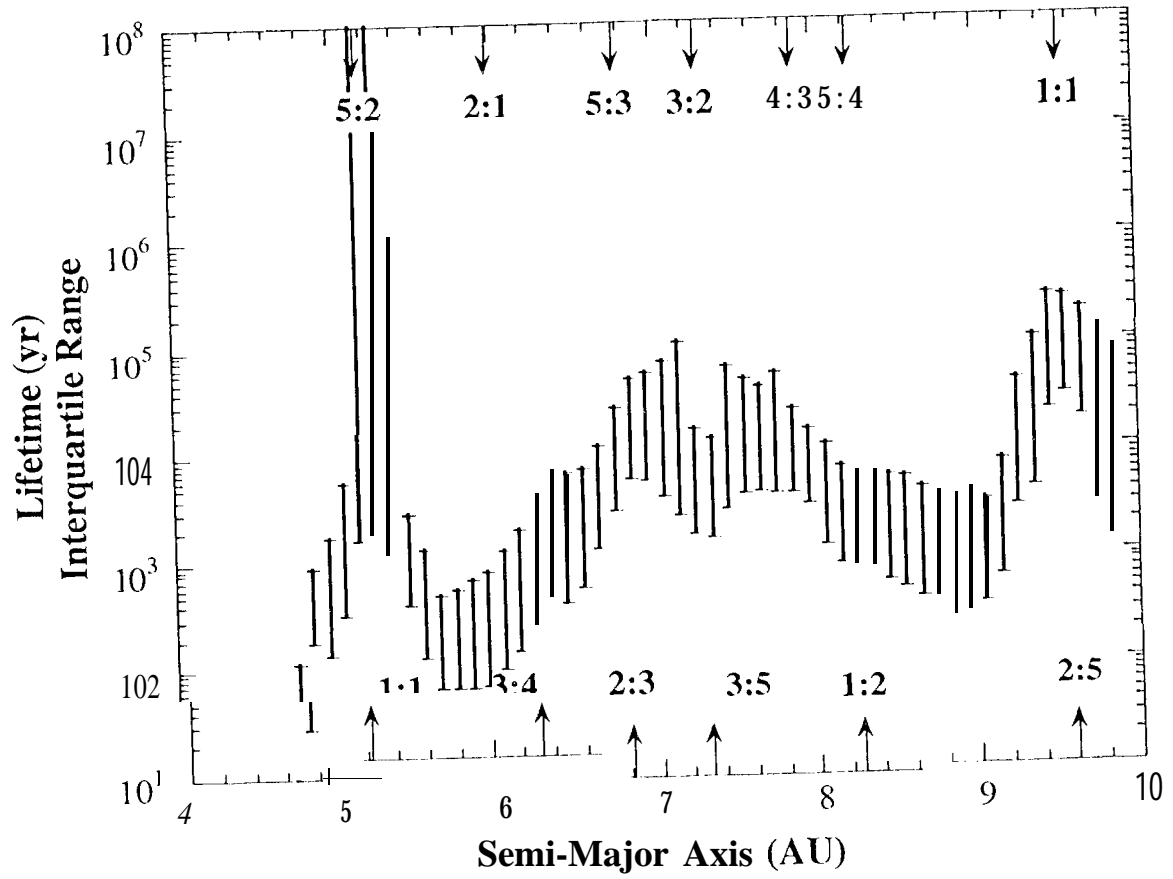


Figure 8

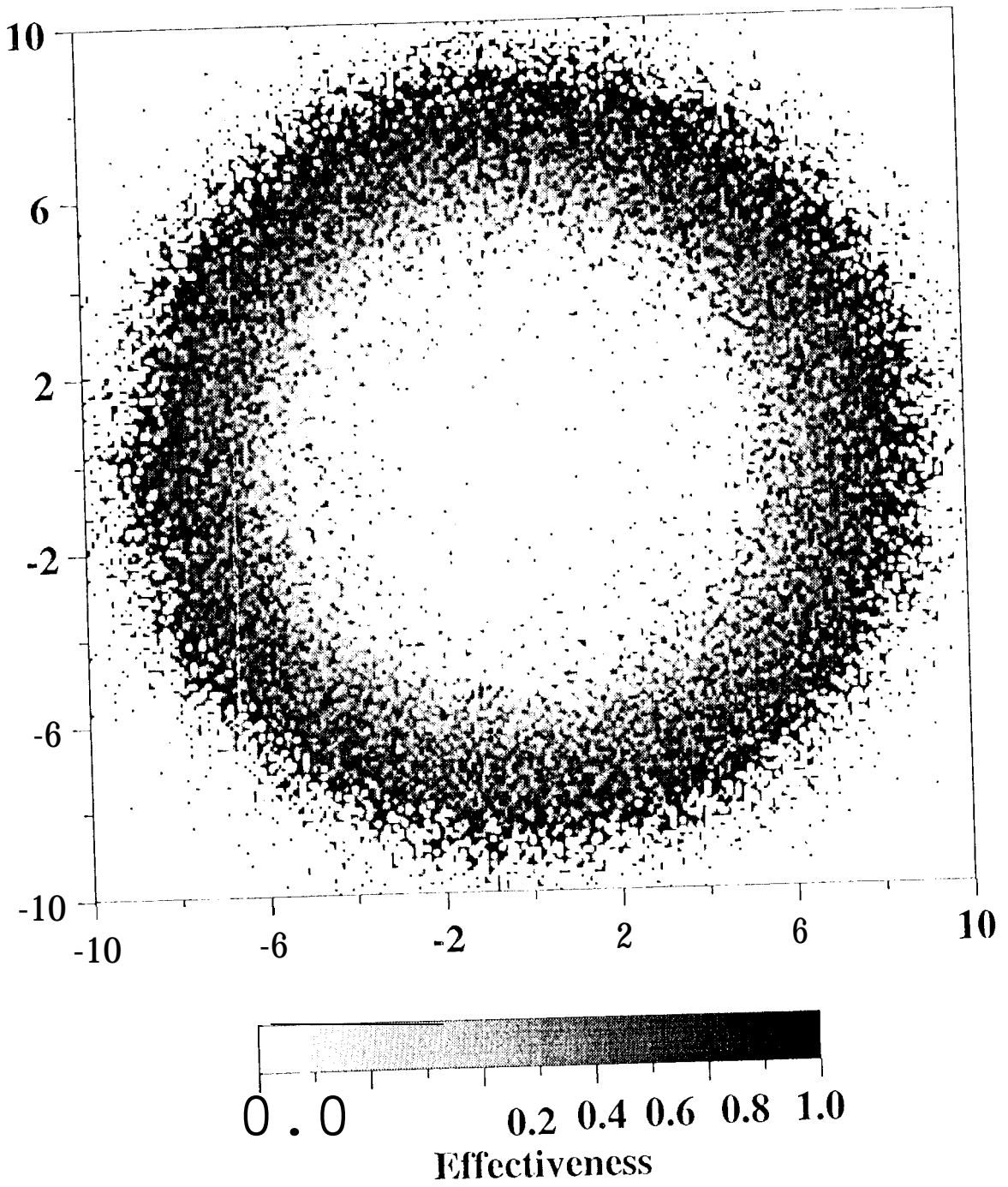


Figure 9

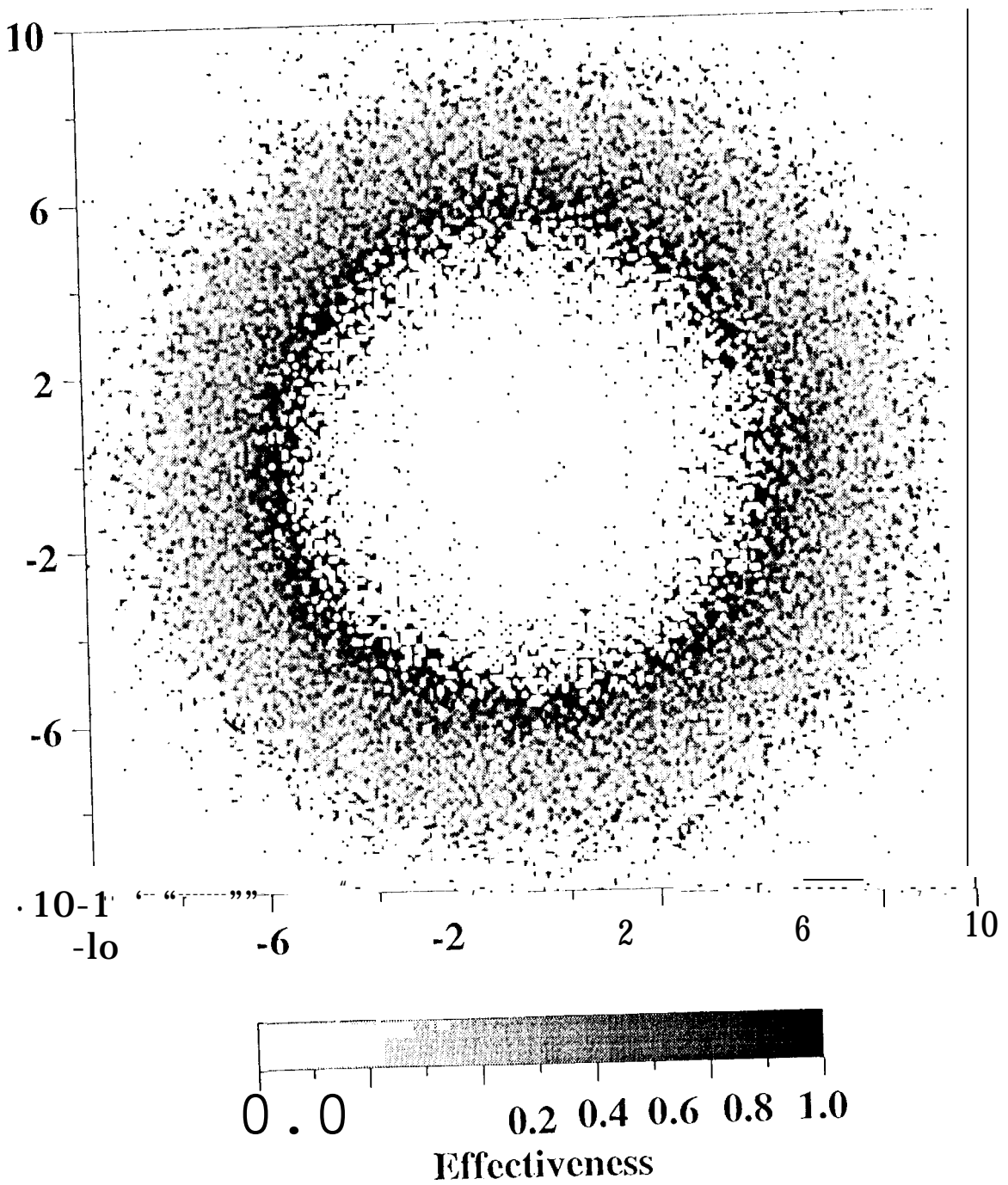


Figure 10

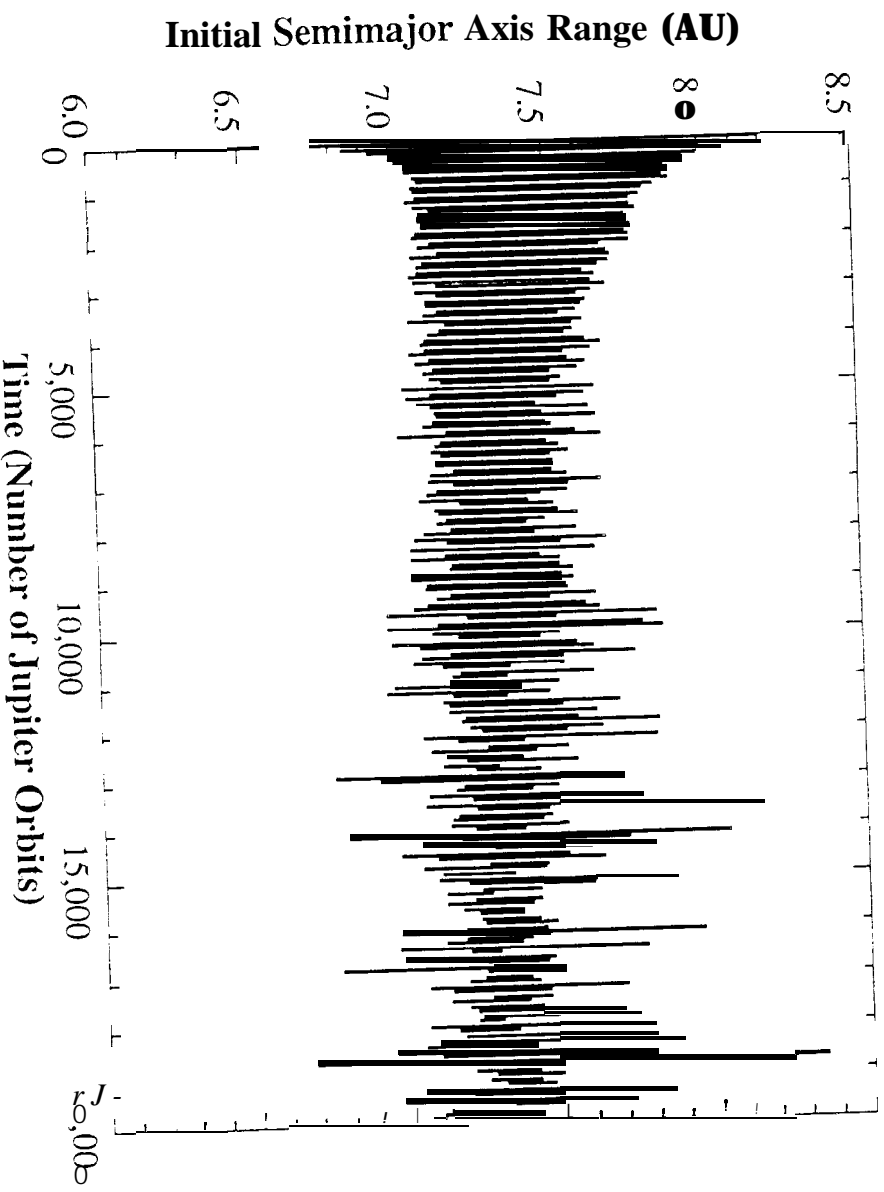


Figure 11

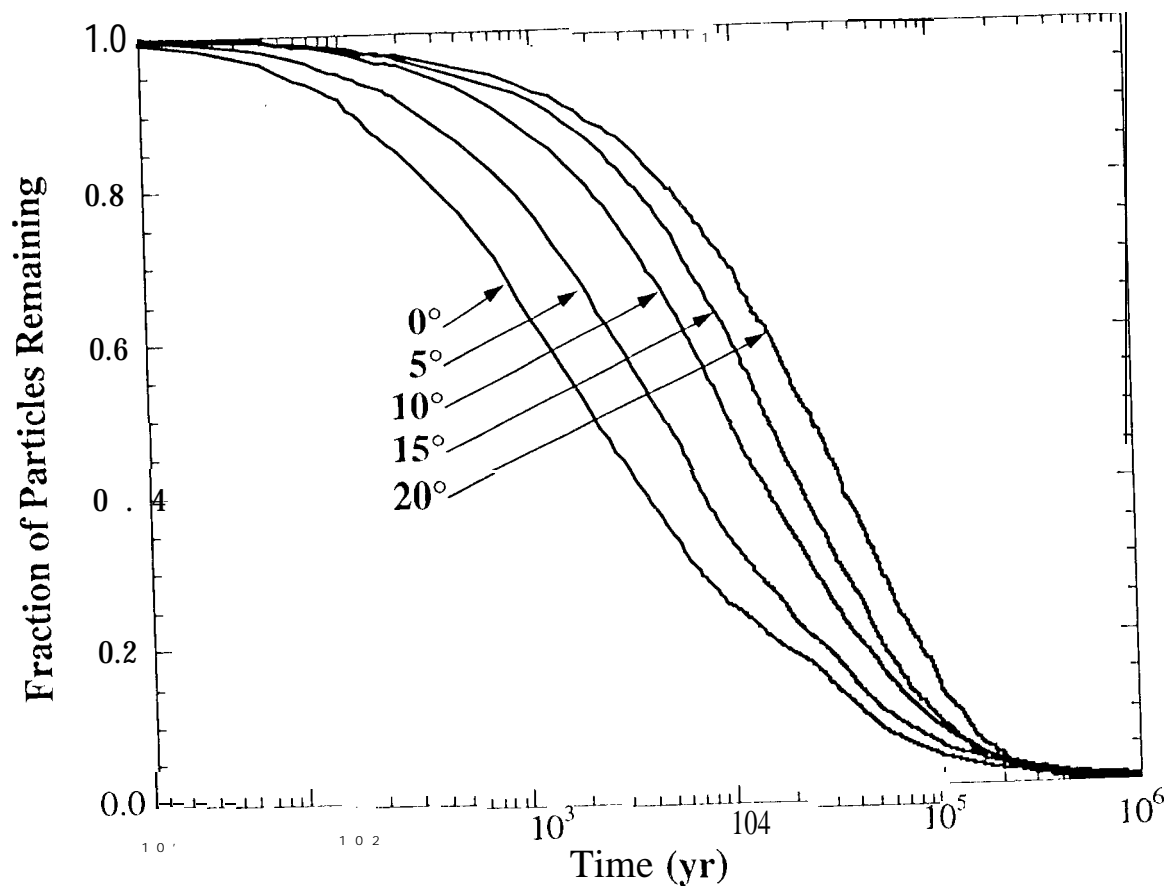


Figure 12

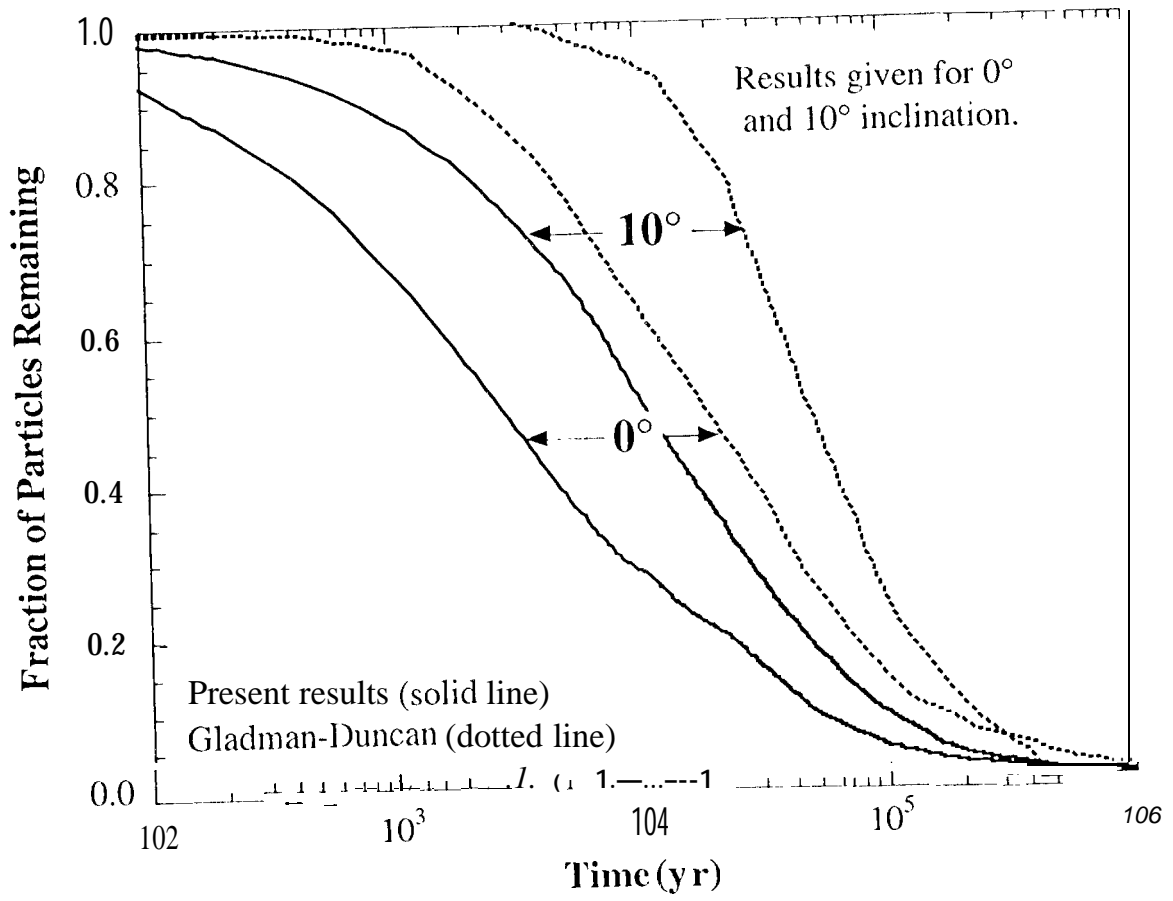


Figure 1.3

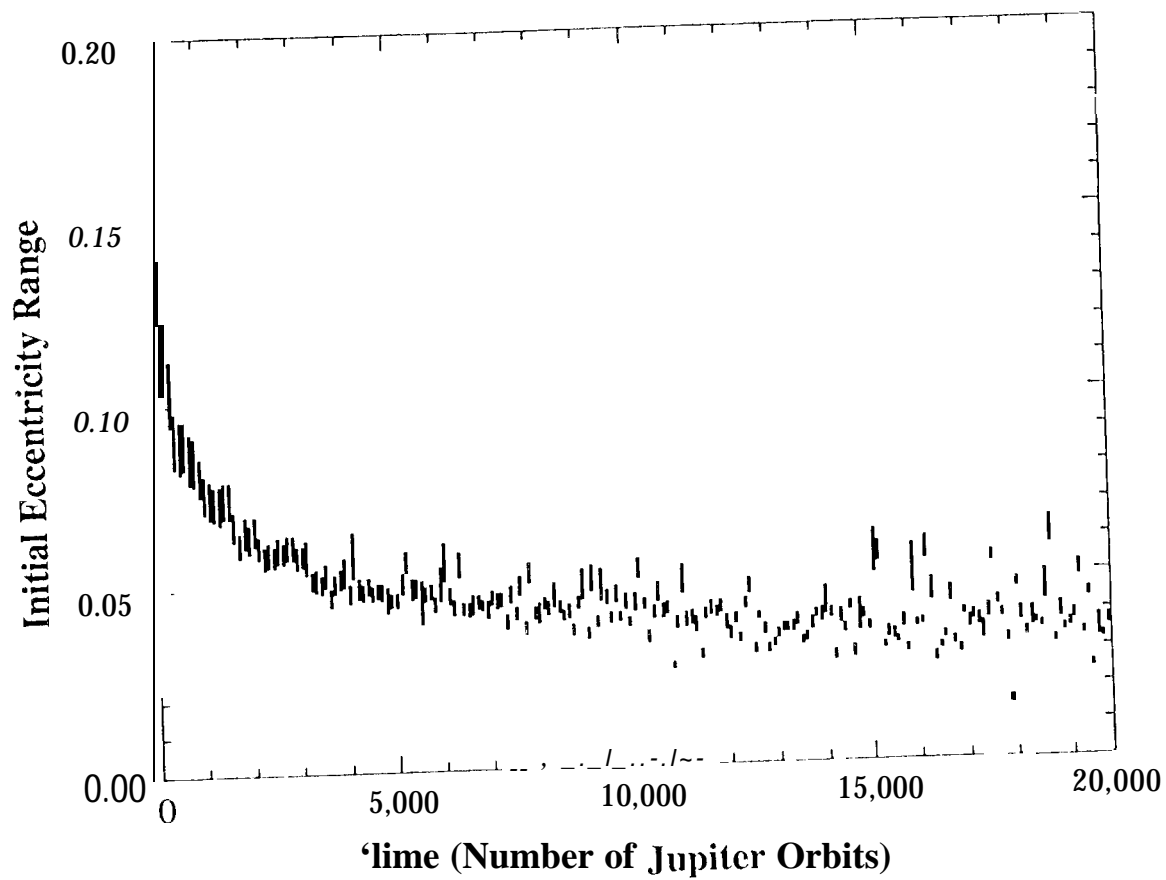


Figure 1.4

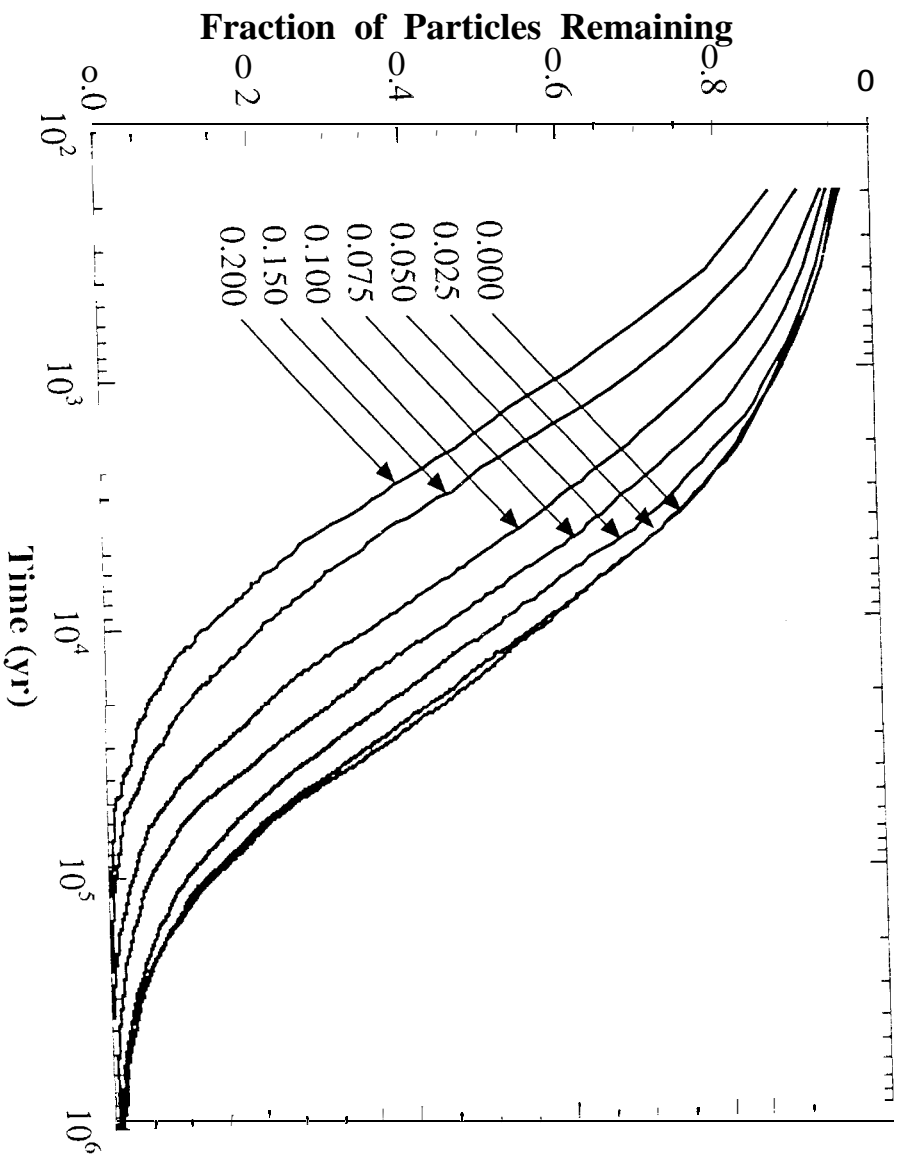


Figure 15

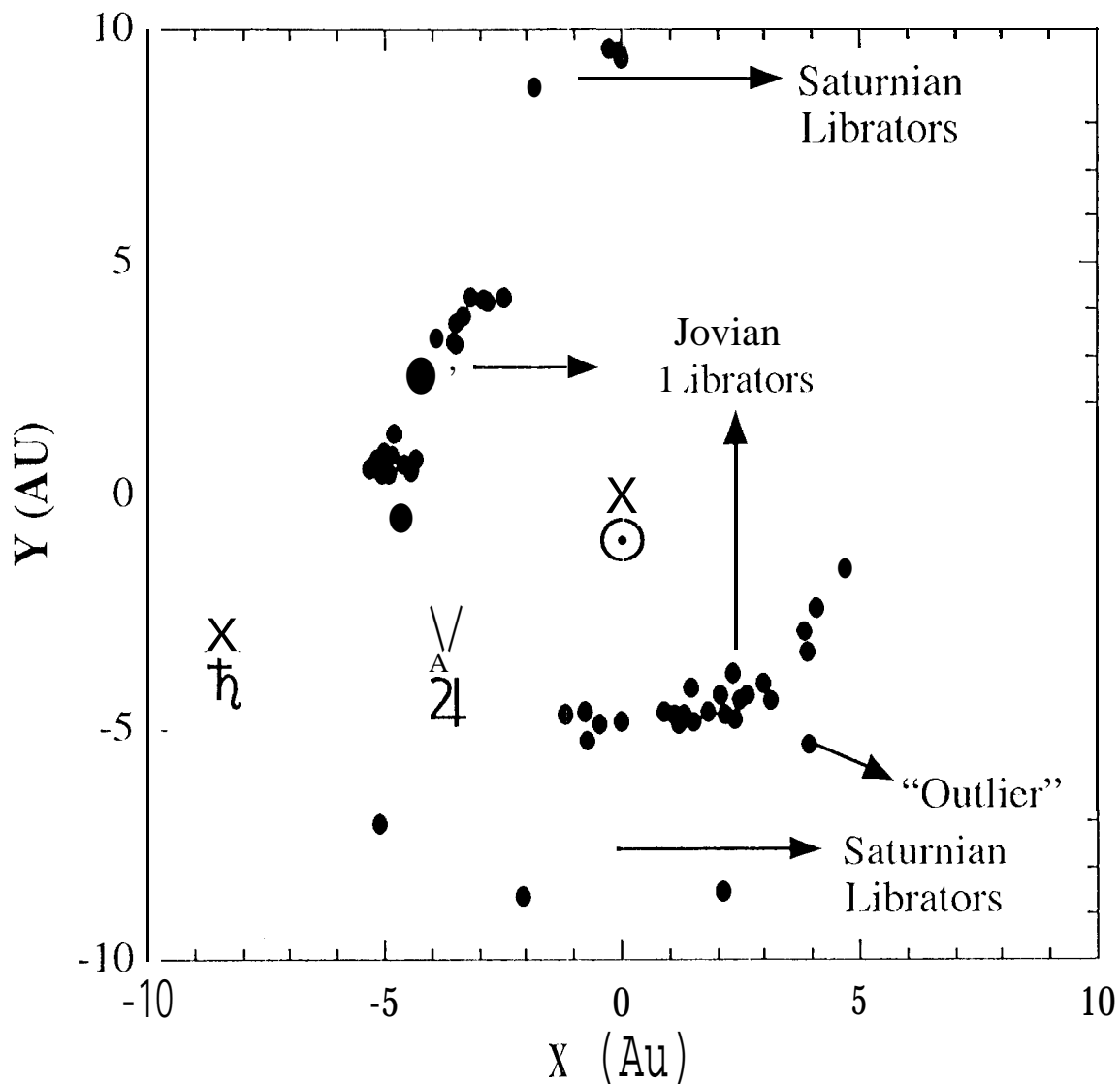


Figure 1.6